NANO-PETROPHYSICS STUDY OF THE THREE FORKS FORMATION IN THE

WILLISTON BASIN, NORTH DAKOTA, U.S.A.

by

DANIEL SAMUEL BAAH

Presented to the Faculty of the Graduate School of

The University of Texas at Arlington in Partial Fulfillment

of the Requirements

for the Degree of

MASTER OF SCIENCE IN GEOLOGY

THE UNIVERSITY OF TEXAS AT ARLINGTON

May 2015

Acknowledgements

     I would like to begin by thanking God Almighty for His strength, love and grace throughout my research project. Special thanks to my supervisor Dr. Qinhong Hu and my other committee members, Dr. John Wickham and Dr. William Griffith for their support and guidance throughout the project.

     I would also like to thank the Ms. Julie LeFever and the staff of the Wilson M. Laird Core and Sample Library and the North Dakota Geological Survey for allowing me to use their facilities, photographs, and samples.

     Lastly, I would like to thank my parents and siblings for their persistent love and support throughout my lifetime of education. Their support in my educational pursuits, their suggestions to improve my work, and also the necessary tools I have needed to succeed in life have ultimately guided me to this point.

April 3, 2015

Abstract

NANO-PETROPHYSICS STUDY OF THE THREE FORKS FORMATION IN THE

WILLISTON, NORTH DAKOTA, U.S.A.

Daniel Samuel Baah, M.S.

The University of Texas at Arlington, 2015

Supervising Professor: Max Qinhong Hu

The Late Devonian Three Forks Formation has increasingly become one of the productive plays in the Williston Basin, North Dakota. This growth has been attributed not only to new drilling and completion techniques but also to the availability of new geological information. Although production in the Three Forks Formation has increased, maximum recovery and overall hydrocarbon production is still limited. According to the North Dakota Industrial Commission, the oil recovery factor in the Three Forks Formation is $8.9 \pm 5.32\%$, so only a small percentage of the original oil in place is being produced.

One of the most challenging aspects of reservoir quality in the Three Forks Formation has been characterizing the permeability, porosity and tortuosity which affect fluid flow and chemical transport in tight rocks. These parameters are macroscopic manifestation of the pore geometry and topology which are not easily accessible because of the dominant nanometer-scale pores. More information is needed with regards to the nanopore size distribution and how the pore connectivity is related to fracture networks.

The mixed siltstone/sandstone/carbonate samples for all of five members of the Three Forks Formation were obtained from well Round Prairie 1-17H from Williams County (API No. 18257). For these tight rocks, we have studied the pore structure, edge-accessible porosity, and wettability using the following complementary tests: mercury

intrusion capillary pressure, tracer imbibition and tracer diffusion into fluid-saturated rock. The latter was done by pulling a vacuum on dry rock followed by the introduction of a tracer-free fluid. These tests use tracer-bearing fluids (API brine or n-decane) to examine the association of tracers with mineral or kerogen phases, followed by elemental analyses with laser ablation-ICP-MS to map out the presence and distribution of tracers inside the rock.

The results from these innovative approaches indicate the limited accessibility and connectivity of nanopores in the samples. In addition, the Three Forks Formation seems to be mostly oil-wetting, with fast imbibition and diffusion for n-decane tracers. The interplay of wettability and connectivity could lead to the steep first-year production decline and low recovery factors because of the limited pore connectivity which inhibits the migration of hydrocarbon molecules in the rock matrix to the stimulated fracture network.

Table of Contents

List of Illustrations

List of Tables

Chapter 1

Introduction

The Three Forks Formation has received renewed research focus in the past few years because of its emergence as an unconventional hydrocarbon reservoir. In unconventional reservoirs, the oil is thought to be trapped in the pores of tight rocks at the sub-micron level. In order to extract this oil in a more economic and efficient manner, it is important to understand the pore-size distribution and the pore connectivity that dictate fluid flow and mass transfer at the sub-micron scale (Nia et al., 2013).

In this research, a study is made on the nano-petrophysics of the Devonian green shale and mixed siltstone/sandstone/carbonate rock of the Three Forks Formation in the Williston basin. The formation which is about 250 feet thick, unconformably underlies the Bakken Formation throughout the Williston basin, covering portions of North Dakota, northwestern portion of South Dakota, northeastern portion of Montana and the southern portions of Saskatchewan and Manitoba (Figure 1-1).

Production in the Three Forks Formation has been from units 5 and 4 which get their source from the organic rich Bakken. The Formation has an estimated average porosity of 6.9% and a recovery factor of 8.93% depending on reservoir characteristics (Nordeng and Helms, 2010) (Table 1-1). The first production recorded in the Three Forks Formation was in the Antelope field in 1953, however, Continental Resources, the largest oil producer in the Williston basin completed the first horizontal well (Mathistad 1-35H) in the Three Forks formation in 2008 (Continental Resources, 2012). Several horizontal wells have also been drilled by other companies such as Whiting Petroleum, Kodiak Oil and Gas, and Brigham Exploration, and most of these horizontal wells have been productive in the Mickenzie, Williams, Dunn, Burke and Mountrail counties which together have a cumulative OOIP of 12.2 billion (Nordeng and Helms, 2010).

1

Although hydrocarbon production in the Three Forks Formation has been successful with horizontal drilling and multi-stage fracture stimulation techniques, questions exist relating to where the hydrocarbon is stored in the rock matrix and what pathways the hydrocarbons take from the rock matrix to the induced fractures that allow them to flow into the well bore.

Exploration of the Three Forks Formation in North Dakota has been combined with the Bakken Formation exploration. The two formations are often considered a continuous, commingled reservoir and are pooled together. The USGS estimates the Bakken/Three Forks play (US only) to contain 7.375 billion barrels of oil, 6.723 trillion cubic feet of gas and 527 million barrels of natural gas liquids. Doubling from an earlier 2008 assessment, the Mississippian/Devonian Bakken is estimated to hold 3.65 billion barrels of recoverable oil, while the Devonian Three Forks formation is estimated to hold slightly more at 3.73 billion barrels of recoverable oil (Roth, 2013).The success of recent wells drilled into the Three Forks Formation of North Dakota has resulted in the re-evaluation of this unit (LeFever et al., 2010) and numerous fundamental questions have been asked about the formation, including what are the nature and distribution of pores that compose reservoirs in the formation. Identification of the pore system has become a higher research priority as the commercial value of the formation rocks has increased. This study shows that much of the rock pore system is not readily observable by conventional sample-preparation methods. Because of their small size, most pores are difficult to differentiate from sample preparation artifacts, as seen in broken or conventionally mechanically polished samples. In order to observe and study pores more accurately, new approaches have been implemented to sample preparation that allows unequivocal recognition of pores as small as 5 nm (Reed and Loucks, 2007).

The objectives of this study are to investigate the pore structure (both geometry and topology) present in the Three Forks Formation and consider the links between pore structure of these formation rocks and hydrocarbon migration, the rocks tortuosity and permeability pathways from the host rock matrix into the induced fracture system.
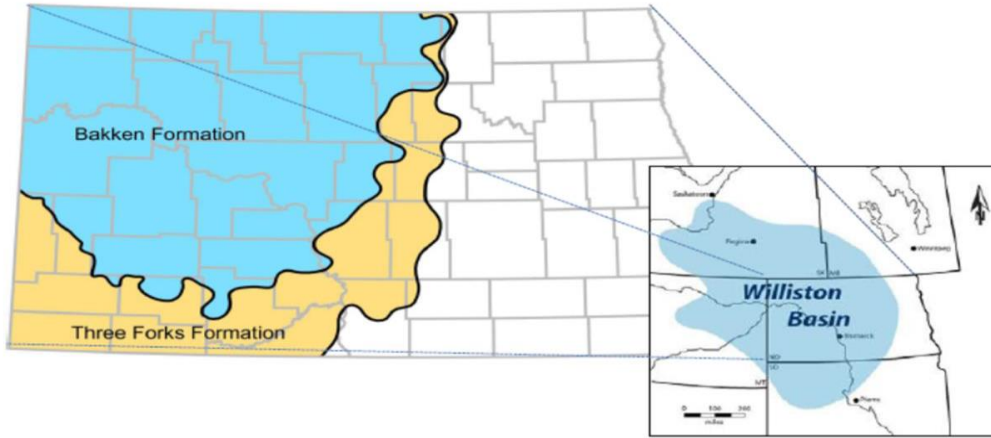
Figure 1-1 Extent of the Three Forks Formation in North Dakota

Table 1-1 Summary statistics obtained from The North Dakota Department of Mineral Resources (DMR) exhibits (modified from Nordeng, 2010).

	Three Forks Formation	Pay Thickness (ft.)	Oil saturation (% pore space)	Porosity (%)	Recovery Factor (%)
	Average	30.5	64.80	6.93	8.90
NDIC Exhibits	Standard Deviation	19.78	11.40	2.33	5.32
	Number of Cases	84	85	85	76

Table 1-1 Location of Study Area

The study area is located in the North Dakota part of the Williston Basin, specifically the Williams County (Figure 1-2). The stratigraphic interval for this research is the Late Devonian Three Forks Formation. Subsurface cores and well log data provided the data needed for this study. The well log data was used to determine the different depths of each unit of the Three Forks Formation.
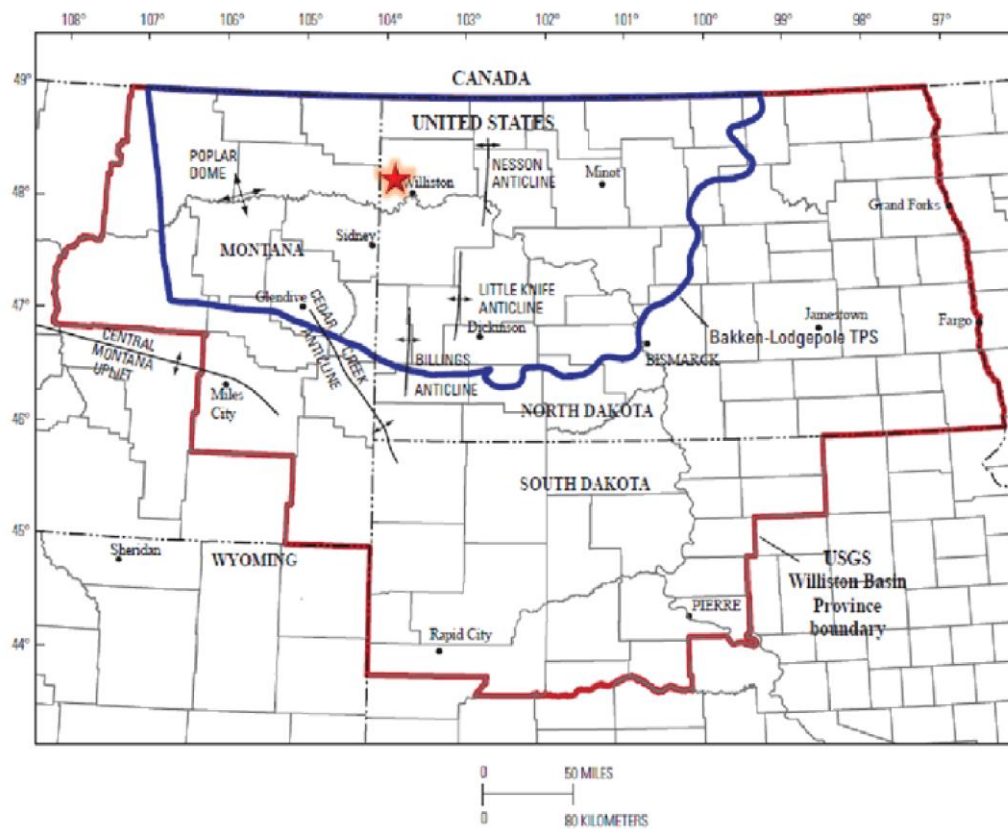
Figure 1-2 Location of the study area. The red star represents the location of well Round Prairie 1-17H.

1.2 Previous Work

There is no previous work on the nano-petrophysics of the Three Forks Formation but there has been similar works in other plays in different basins in the country. Different approaches have been employed to study and characterize the pore structure and fluid flow in rocks. Contrary to conventional gas reservoirs, fluid flow in unconventional reservoirs is controlled by free gas flow, desorption, diffusion, and imbibition suction mechanisms. Free gas flow can be a non-Darcy type in both organic and inorganic matrices as a result of the slippage effect, but a Darcy type in natural and hydraulic fractures (Wang et al., 2009).

Mercury-injection capillary pressure (MICP) has been the preferred method for characterizing the pore-throat structure of unconventional reservoirs (Comisky et al., 2007), and low-pressure gas adsorption methods have also been used (Bustin et al., 2008a). Compared to other pore system characterization approaches (e.g. gas sorption), mercury-injection capillary pressure is based on a simpler principle and covers a wide range of pore sizes (from 3nm to 300 µm), which makes it a powerful characterization tool. Recently, small-angle and ultra-small-angle neutron scattering techniques have also been applied to characterize the pore system of tight gas and shale reservoirs (Clarkson et al., 2012a). Additionally, Hu et al. (2,012) characterized the pore connectivity of natural rocks using spontaneous water imbibition, tracer concentration profiles, and imaging in combination with network modeling. An empirical equation was proposed using median pore throat radius to calculate permeability, which is an important hydraulic parameter in porous media (Gao and Hu, 2013).

Finally, Bryant et al. (2014) worked on the effect of pore structure on the producibility of tight-gas sandstones. According to them, ultimate recovery is dependent

5

on the connectivity of natural fractures and the pore structure of the rock matrix. They analyzed lab measurements that were indicative of the pore structure, and predicted the effect of pore structure on producibility. In addition, they developed a relationship between the EUR of tight-gas sandstones and their petrophysical properties measured by drainage and imbibition tests (mercury intrusion, withdrawal, and porous plate) and by resistivity analyses. They concluded that a better understanding of the pore structure of unconventional rocks affects hydrocarbon productivity since well-connected pores tend to have better permeability.

Chapter 2

Geologic History

2.1 Williston Basin Structural History

The Williston Basin is of the Early Paleozoic age, it is a large and roughly circular intracratonic depression that developed on the North American craton (Kerr, 1988; Pitman et al., 2001). It is bounded by the Canadian Shield to the north and east; the Alberta shelf, Little Rocky Mountains, and the Black Hills to the west; and the Trans-Continental Arch to the south (McCabe, 1957).The geographic area of the basin is about 300,000 mi^2 and it includes portions of North Dakota, South Dakota, Montana, and adjacent Canadian Provinces of Manitoba and Saskatchewan. (Figure. 2-1; Pollastro et al., 2010). During the Precambrian, the Archean Superior craton was sutured to the Archean Wyoming craton by the Trans-Hudson Belt which resulted in a collision, creating a north–south trending strike-slip fault and shear belt (Figure 2-2; Anna et al., 2011). A basin center was then created by later folding of the Trans-Hudson orogenic belt and rifting (Green et al., 1985a).

Subsidence of the basin is interpreted as a result of convection current movement and thermal processes that expanded and uplifted the lithospheric crust and created complex variations of thickening, cooling, and erosional truncation (Crowley et al., 1985). The basin is commonly viewed as structurally simple because of its nearly complete stratigraphic section, with most units thinning from basin center to basin edge, and the faults and other structural features commonly having only a small net displacement or movement. Detailed studies reveal however, a more complex tectonic history due mostly to the deformed underlying basement rocks and two major bounding structural fault systems (Figure 2-1) responsible for much of the basin's interior faults and lineaments, block-fault movements, sedimentation patterns, salt dissolution, fluid

7

movement, and thermal history (Green et., 1985; Brown et al., 1987; Gerhard et al., 1988). Major structural features present in this basin are the Nesson and Cedar Creek anticlines. Smaller structural features include the Antelope, Billings, Little Knife, and Poplar anticlines (Figure 2-3). The Cedar Creek Anticline flanks the southwestern edge of the basin and to the northeast. This structure has undergone five major periods of growth during the Early Devonian, Late Devonian, Late Mississippian, Triassic and post Pliocene time (Clement, 1976). Several upper Paleozoic sedimentary changes also occur in the vicinity of this anticline due to the thinning or absence of Devonian and Silurian rocks along the crest of the anticline. The Nesson, Billings and Little Knife antilcines all trend north except for the Poplar Dome which has a northwest trend.

Deposition of sediments began in the Williston Basin during Cambrian time, but subsidence and basin filling were most intense during the Ordovician, Silurian, and Devonian Periods, when thick accumulations of limestone and dolomite, with lesser thicknesses of sandstones, siltsones, shales, and evaporites were deposited. Subsidence continued on a reduced scale into the Mississippian and ended by Pennsylvanian time (Figure 2-4). Regional subsidence returned during the Mesozoic Era, although total sediment thicknesses were much less than during the Paleozoic. Due to an erosion dominated period of subsidence, marine sediments were not deposited in the basin continuously. However, some of the rocks from the Phanerozoic time were preserved in the basin. These strata records several cycles of marine transgression that filled the basin, followed by marine regressions that drained the basin. A widespread and significant erosional unconformity marking the end of the Devonian represents a period of uplift and continued until the Mississippian time. It is this event that has mostly affected the deposition, reworking and erosion of the Three Forks Formation.
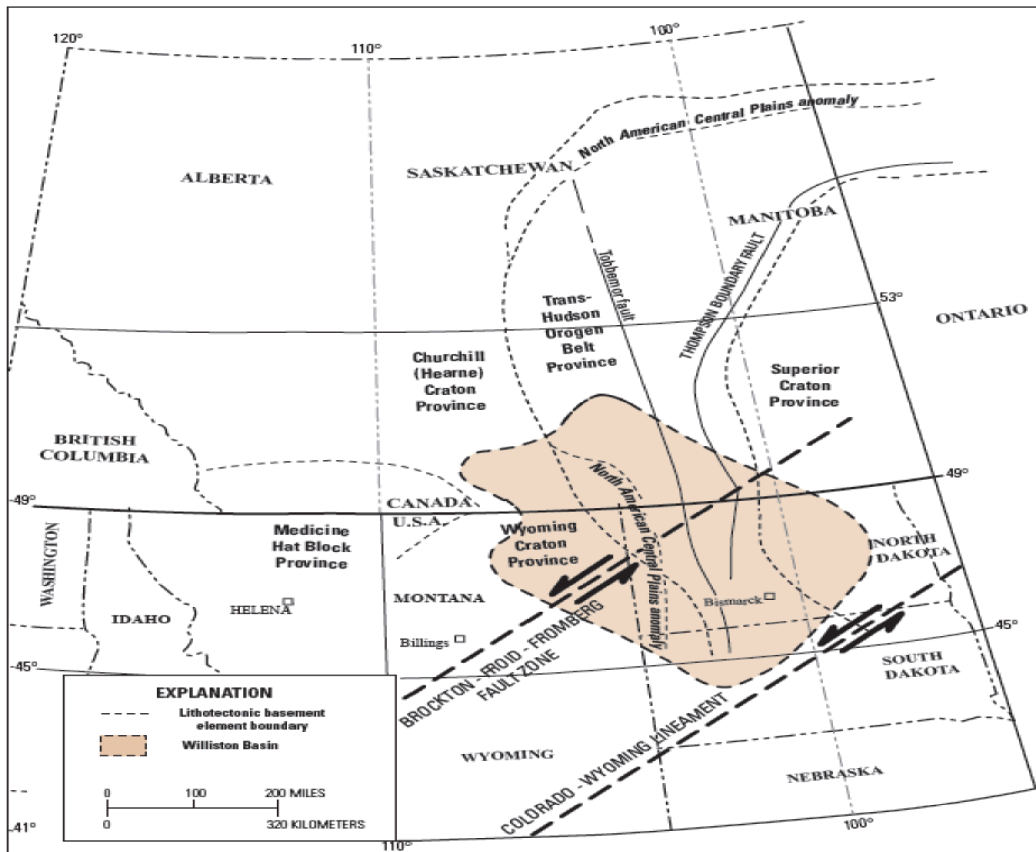
Figure 2-1 General extent of Williston Basin showing two major fault systems responsible
for the formation of the basin (modified from Pollastro et al., 2010).
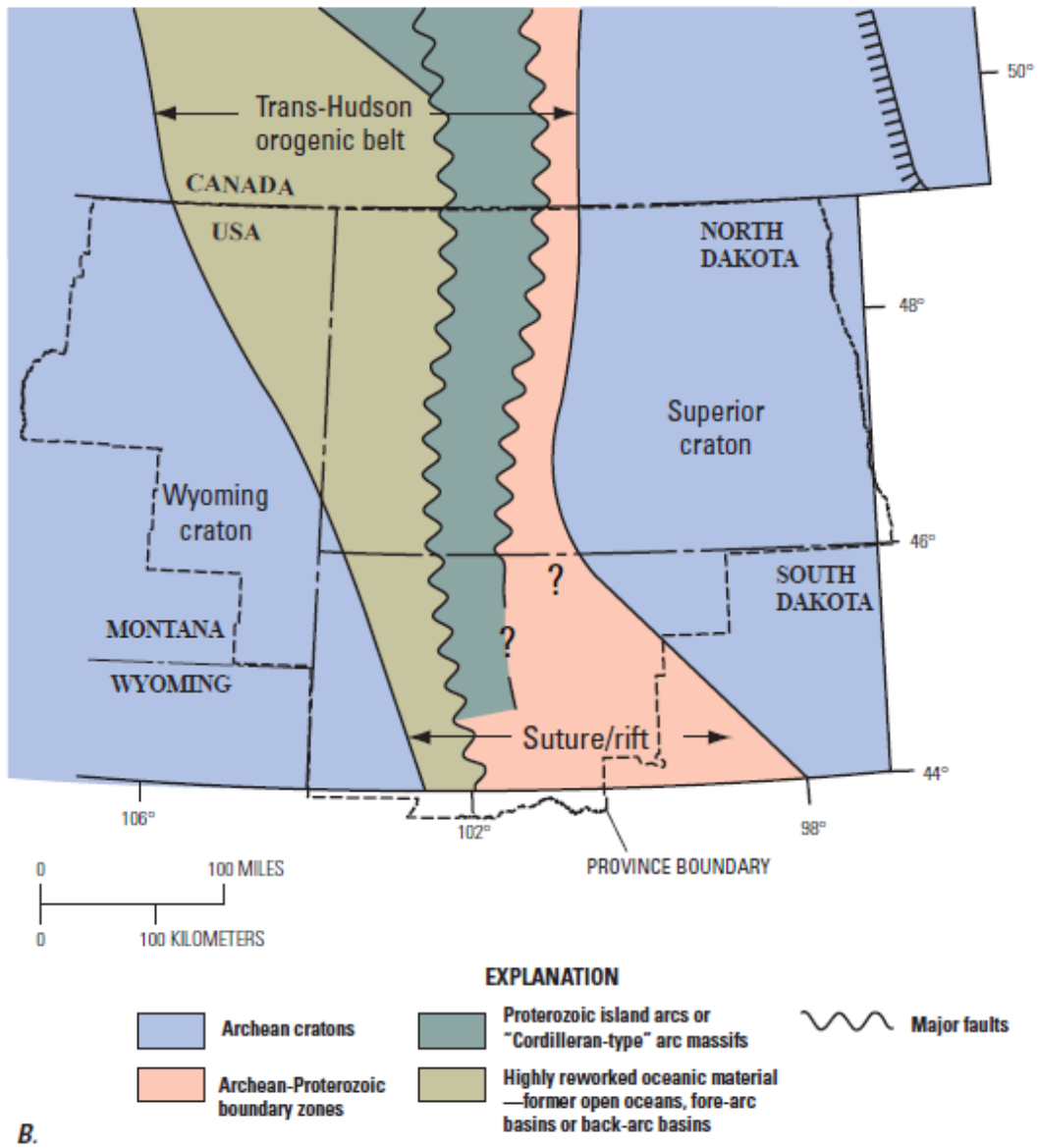
Figure 2-2 Configuration of the Trans-Hudson orogenic belt and associated north–south trending structures of the Williston Basin (modified from Nelson et al., 1993).
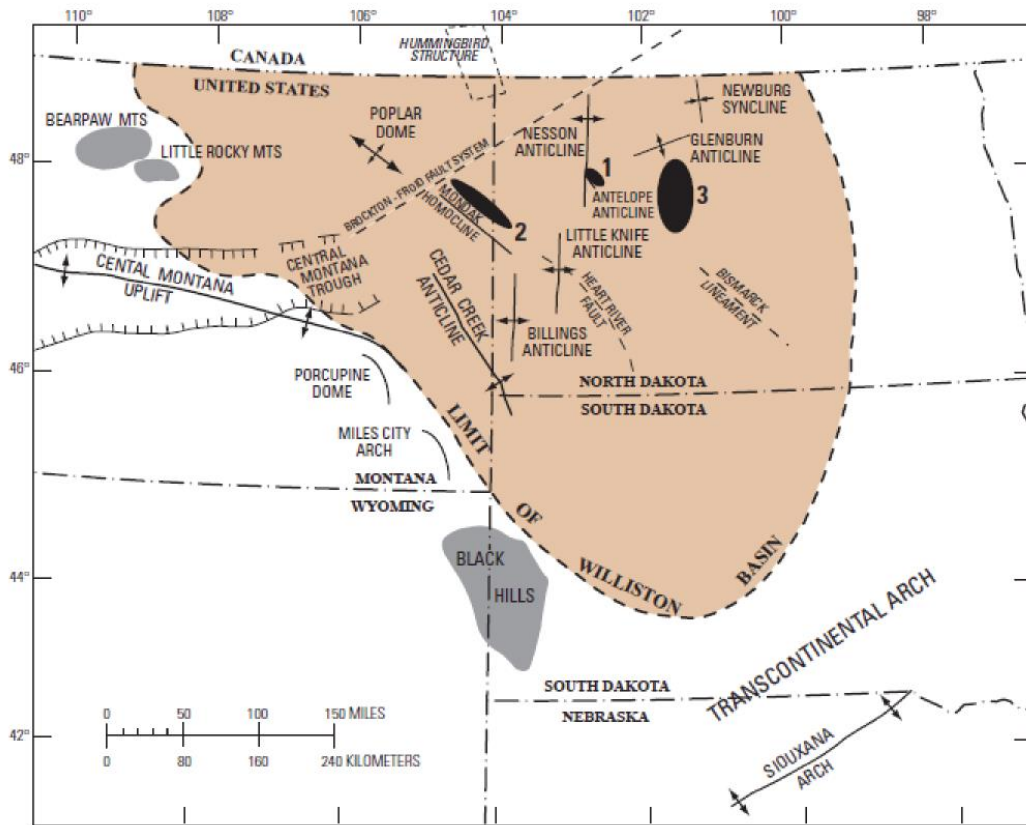
Figure 2-3 Present-day major structural elements of the U.S. portion of the Williston

Basin. Solid black ovals show general location of three major areas of oil production:

Antelope field (1), Elm Coulee field (2), and Parshall and Sanish fields (3) (from Pollastro,

2013).

2.2 Regional Stratigraphy and Sedimentology of the Williston Basin

The Williston basin has undergone relatively mild tectonic distortion during the

movement of Precambrian basement blocks (Gerhard et al., 1982). This mild tectonic

movement combined with the relative sea level changes along with the local and regional

structural episodes influenced the cyclic nature of the sedimentary deposition in the

basin. The basin itself contains nearly 16,000 feet of sedimentary rocks ranging from the

Cambrian to the Tertiary. There are six major depositional sequences, each bounded by major unconformities (Sloss, 1984) in the basin. They are from oldest to youngest, the Sauk, Tippecanoe, Kaskaskia, Absaroka, Zuni, and Tejas sequences (Anna et al., 2011) (Figure 2-5).

The Sauk major sequence consists of the Upper Cambrian Deadwood Formation, which represents the initial stages of a major first-order transgression over a low-relief Precambrian surface. The sediment source for the Deadwood was from weathered Precambrian rocks, eroded from highlands to the east or from the transcontinental arch to the southeast (Carlson and Thompson, 1987). Depositional environments of the Deadwood include shallow marine, coastal plain, and rare alluvial plain, with successions of sandy carbonate, mudstone, siltstone, and quartz arenites (burrowed and nonburrowed). Several minor transgression-regression cycles separate the Deadwood Formation into multiple members (LeFever, 1996).

The Tippecanoe major sequence marks the start of the second transgression-regression cycle, and also marks the beginning of Ordovician sedimentation (Anna et al., 2011). The Winnipeg Group was deposited as a succession of shallow marine sandstone, shale, and shaly carbonate during the initial transgression. It unconformably overlies the Deadwood except in the eastern part of the basin where it rests on Precambrian basement (Anna et al., 2011). Overlying the Winnipeg conformably is the Red River Formation which represents the initial unit that was deposited during numerous cycles of shallow marine carbonate and anhydrite and salt sedimentation. The Stony Mountain and Stonewall Formations and the Interlake Group conformably overly the Red River. Third and fourth order cycles in these strata continue the pattern of cyclic sedimentation, consisting of subtidal limestone, intertidal dolomite and dolomitic limestone, and peritidal or supratidal anhydrite or salt (Anna et al., 2011).

The Kaskaskia major sequence exhibits a range of depositional environments, including subtidal, intertidal, and rare supratidal with various percentages of dolomite, limestone, salt, and anhydrite (Anna et al., 2011). The Kaskaskia begins with a second-order transgressive event in the Early Devonian and concludes as a major regression at the end of the Mississippian. During this time the basin was subjected to restricted marine conditions that were followed by episodes of regular circulation due to sea level change. This produced a variety of lithologically different formations in the sequence. During the initial transgression, the Ashern and Winnipegosis Formations overlain by the Prairie Formation were deposited. The Prairie Formation is dominated by evaporites and minor clastics, representing a period of regression and restricted water flow (Anna et al., 2011). A second transgression occurred and deposited the Dawson Bay Formation. Due to later sea level regression, the Souris River, Duperow, Birdbear, and Three Forks Formations were deposited. The Three Forks Formation includes cyclical sequence of dolomitic claystone and mudstone, interbedded siltstone and will be discussed in the following sections. The third transgression occurred during the late Devonian, resulting in the deposition of the highly organic-rich Bakken Formation (Anna et al., 2011). As the sea level receded, there was a reduced clastic sediment input into the basin and the Mississippian Lodgepole Limestone was deposited in subtidal conditions resulting in low porosity limestones (Anna et al., 2011). The Madison Group was deposited above the Lodgepole Formation and represents a time with minor transgression-regression cycles. At the end of the Mississippian the Big Snowy Group was deposited, overlaying the Madison Group. The Big Snowy Group consists of interbedded sandstones, shales, and limestone. This regression ended major Paleozoic marine sedimentation in the Williston Basin, with exception of the Pennsylvanian and Permian (Anna et al., 2011).

The Absaroka major sequence lasted from Pennsylvanian to Triassic. It includes several secondary transgressive and regressive cycles in a relatively low sea level environment (Anna et al., 2011). The rock sequence includes interbedded sandstone, siltstone, shale, and limestone of the Pennsylvanian Tyler Formation and equivalents; the overlying Minnelusa Formation records input from the Ancestral Rocky Mountain orogenic belt and the transcontinental arch. The sediments were deposited in alluvial plains, as well as in near shore and shelf environments from prograding delta systems and in barrier island environments (Sturm et al., 1982).

The Zuni major sequence represents Jurassic and Cretaceous strata that were deposited as a first-order cycle. The major sequence also represents a lithogenetic package bounded by regional unconformities. The rocks here are identical to the rocks of the upper part of the Absaroka sequence, with successions of light-colored sandstone and siltstone and minor carbonate and salt. (Anna et al., 2011). Marine subtidal and intertidal environments deposited anhydrite and salt at the basin center during the Jurassic. By the end of the Jurassic the lithology switched to continental sandstone and mudstone. In the Lower Cretaceous the lithologies are mostly sandstone, siltstone, mudstone, and shale (Anna et al., 2011). The Upper Cretaceous consists of four major transgression-regression cycles with the same lithology as the Lower Cretaceous.

The Tejas major sequence represents the final first-order regression in the sedimentary history of the Williston Basin. It comprises three regional transgression-regression cycles with strata ranging in age from mid-Paleocene through Quaternary and consisting of continental gravel, sandstone, siltstone, mudstone, and low-grade coal (Anna et al., 2011).

2.3 The Three Forks Formation Stratigraphy

The Late Devonian Three Forks Formation is the focus of this study. The Three Forks Formation is roughly 250 feet thick and it comprises a cyclical sequence of dolomitic claystone and mudstone, interbedded siltstone. Dolomitic siltstones are tan brown, while claystones and mudstones exhibit colors from gray/green to red. The reddish color can result from erosion, weathering and oxidation. This association of very fine-grained lithology is stacked in cyclic patterns, which is evident in cores as well logs, especially the gamma ray (Gutierrez and Sonnenberg, 2013).The Three Forks Formation is formally divided into five units of which Units 4 and 5 are the primary producing units. The units are divided based on sedimentary characteristics and geophysical-log signatures with each unit representing a single coarsening upward cycle (Figure 2-5).

Unit 5 is the uppermost and it consists of a basal thin, massive, tight greyish-green dolomitic shale to silty shale sequence overlain by a greyish-green with light brown to tan dolo-arenitic siltstone clasts with a brecciated appearance (Nicholas et al., 2002). This is overlain by a sequence of light brown to tan dolo-arenitic siltstone and greyish-green shale.

Unit 4 consists of randomly alternating cycles of light brown to tan dolo-arenitic siltstone clasts in a shale matrix, rhythmically alternating laminated siltstone and shale beds, and massive greyish-green to rusty brown shale to silty shale. The shale is overlain by a light brown to tan dolo-arenitic siltstone with greyish-green shale as laminae, interbeds and matrix. It is capped by a thin, massive, tight greyish-green dolomitic shale to silty shale (Nicolas et al., 2005). Sedimentary structures in this unit include ripple marks, trough crossbedding, load structures, escape structures and soft-sediment deformation features (Nicholas et al., 2002).

Unit 3 consists of a blocky, faintly mottled, and reddish-brown to greyish-green dolomitic claystone and mudstone with minor thin, light brown, dolomitic siltstone laminae and rhythmites. It is generally oxidized and reddish-brown in colour but includes redox haloes of light brown in the siltstone to greyish-green in the claystone and mudstone (Nicholas et al., 2002).

Unit 2 consists mostly of concentrated breccia with rotted dolomite fragments in a brown mudstone matrix (Nicholas et al., 2002).

Unit 1 is the lowermost unit and it lies conformably on the Birdbear Formation. It is the most weathered and consists of a thin, basal, brownish dolostone with overlying interbedded reddish-brown to light brown dolomitic siltstone and reddish-brown to greyish-green dolomitic claystone and mudstone. The proportion of siltstone to claystone and mudstone is variable, but siltstone is generally predominant. Disseminated pyrite or iron oxides are common within the mudstone and claystone; white, pink and grey-blue anhydrite occurs as occasional blebs, nodules and fracture fills (Nicholas et al., 2002).
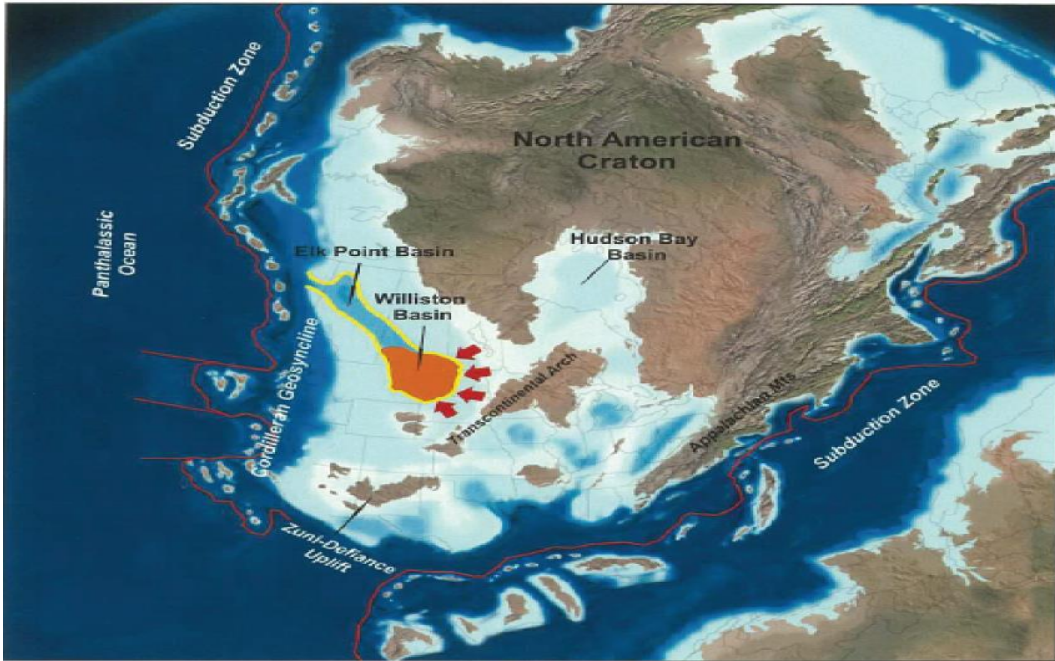
Figure 2-4 Paleogeographic map of Williston Basin during the Late Devonian. Red arrows

indicate direction of clastic sediment transport into the Williston Basin (modified from

Blakey, 2005).
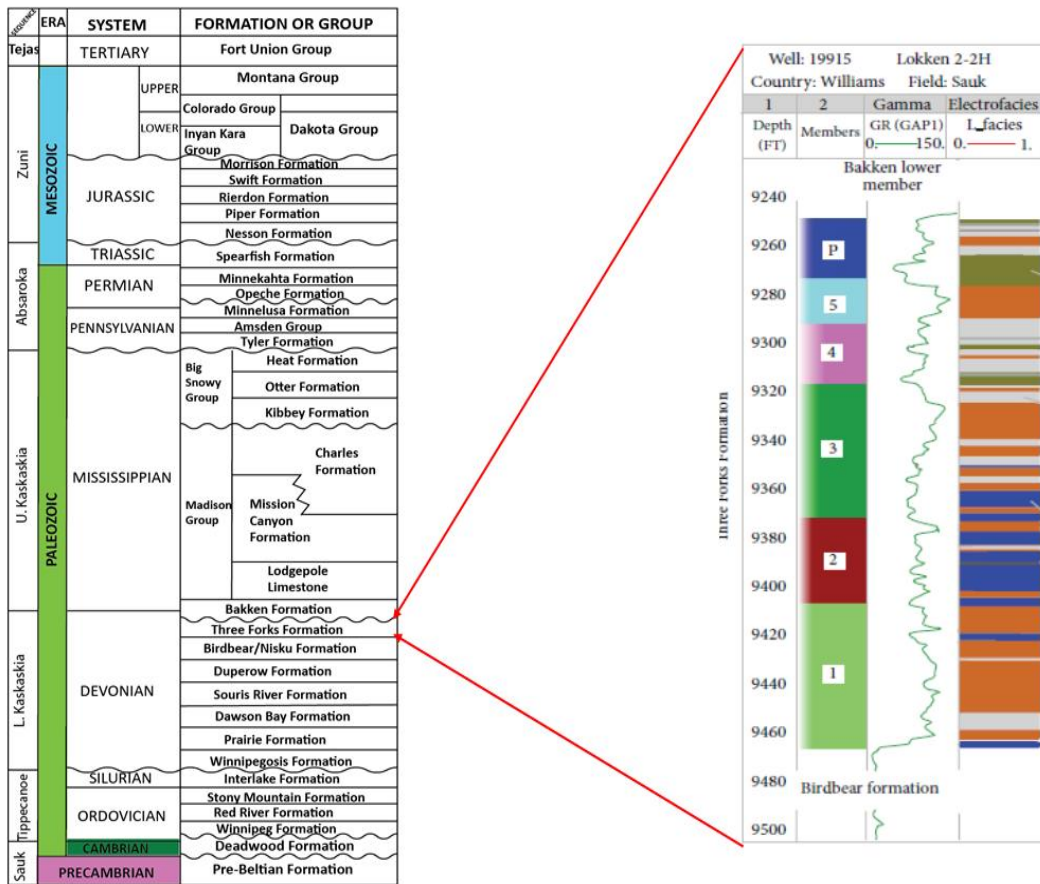
Figure 2-5 Generalized Precambrian to Mesozoic stratigraphic column of the Williston

Basin showing the main unconformities and the Three Forks Formation Units 1-5

(modified from Ashu, 2014).

Chapter 3

Methods

3.1 Sampling Procedure

The sample definitions and determination were based on the direct observation and description of lithology and sedimentary structures on core samples and published data including excellent quality photos from the North Dakota Geological Survey web page (Figure 3-1). The focus of this research is the producing Three Forks interval, but with the purpose of having a complete understanding, samples were procured for all the units of the entire formation. Samples were secured from each of the five units of the Three Forks Formation at different depths from the well Round Prairie 1-17H from the core laboratory of North Dakota Geological Survey located on the campus of the University of North Dakota.

For the purpose of this study, the collected samples were cut into 1-cm-sized cubes. Once the samples are ready, the following laboratory experiments were performed on them;
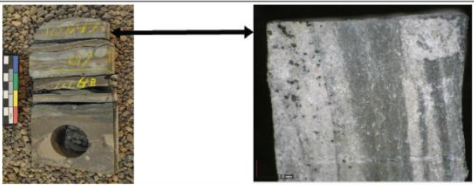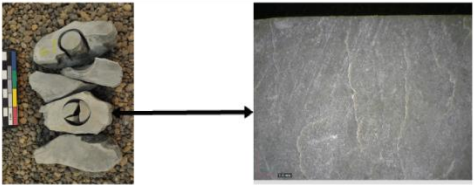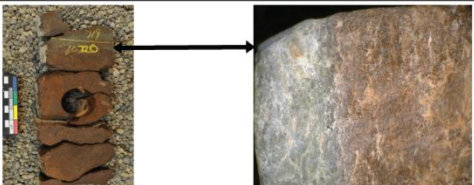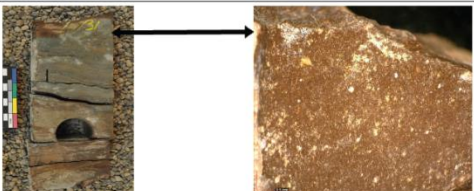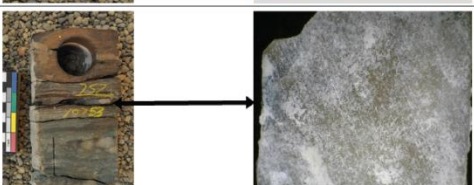
Sample	Rock Description	Depth (ft.)	Sample Photography
Three Forks Unit 5	Thin, massive, tight grey-green dolomitic shale to silty shale.	10647.0	
Three Forks Unit 4	Light brown to tan doloarenitic siltstone clasts in a shale matrix.	10667.0	
Three Forks Unit 3	Massive oxidized silty shale.	10720.0	
Three Forks Unit 2	Concentrated breccia with rotted dolomite fragments in a brown mudstone matrix.	10731.5	
Three Forks Unit 1	Light brown to tan doloarenite with grey green shale to silty matrix.	10753.5	

Figure 3-1 Rock sample description and photographs of the Three Forks Formation units from Well Round Prairie 1-17H.

3.2 Mercury Injection Capillary Pressure (MICP)

The pore system of the samples was analyzed using the mercury injection capillary pressure shown in Figure 3-2, which is applicable to pore-throat size measurements from 3 nm up to 300 μm in diameter. The approach of MICP can also indirectly evaluate other pore characteristics, such as total pore surface area,

permeability, and tortuosity. Mercury is a non-wetting fluid and will therefore not invade

pores unless an external pressure is applied. This external pressure corresponds to the

Washburn Equation (p · r = -2 ·γ·cosθ, where r is the radius of the pore where mercury

intrudes, γ is surface tension of mercury and θ is the contact angle of the mercury on the

surface of a solid sample). The diameter of the pore-throats invaded by mercury is

inversely proportional to the applied pressure; the higher the applied pressure, the

smaller are the pore-throats invaded by mercury. With the increase of applied pressure

during the intrusion process, the volume change of intruded mercury will be recorded by

MICP as an intrusion curve and the pore throat size distribution can be derived from this

intrusion curve according to Washburn's equation.

with Each sample was oven-dried at 60 °C for at least 48 hours to remove

moisture, and then cooled to room temperature (~23°C) in a desiccator with less

than10% RH before the MICP test. Samples were then evacuated to 50 µmHg (0.05 torr,

0.000972 psi, or 6.7 Pa). During the MICP test, each sample was subjected to low-

pressure and high-pressure analyses. The high pressure analysis measured pore-throat

diameters down to 3 nm which corresponds to 60,000 psia (413 MPa) produced by the

Micromeritics AutoPore IV 9510 (Figure 3-2).The low pressure analysis measured pore-

throat diameters down to about 300 µm. Time to allow for equilibrium was 50 seconds

before continuing to the next pressure level.

As reported by Gao and Hu (2013), porosity of the samples can be directly

obtained through the MICP procedure's raw data. Permeability however, is calculated

using the equation of Katz and Thompson (1986; 1987).

$$k = \frac{1}{89}(L_{max})^2(\frac{L_{max}}{L_c})\emptyset S(L_{max})$$

own where k is air permeability (darcies); L_{max} (µm) is the pore-throat diameter at

which hydraulic conductance is maximum; L_c (µm) is the characteristic length which is the

pore-throat diameter corresponding to the threshold pressure P_t (psia) and P_t is

determined at the inflection point of the cumulative intrusion curve; $\emptyset$ is porosity; $S\ (L_{max})$

represents the fraction of connected pore space composed of pore width of size L_{max} and

larger. MICP can also measure the tortuosity of the rocks, Tortuosity is an important

parameter that can help determine rock pore connectivity, which can be derived from the

MICP data using;

$$\tau = \sqrt{\frac{\rho}{24k(1+\rho V_{tot})} \int_{\eta=r_c,min}^{\eta=r_c,max} \eta^2 f_V(\eta)d\eta}$$

Where ρ is

fluid density (mass/volume); k is permeability (area); V_{tot} is total pore volume

(volume/mass); $\int_{\eta=r_c,min}^{\eta=r_c,max} \eta^2 f_V(\eta)d\eta$ is pore-throat volume distribution by pore-throat size.

22
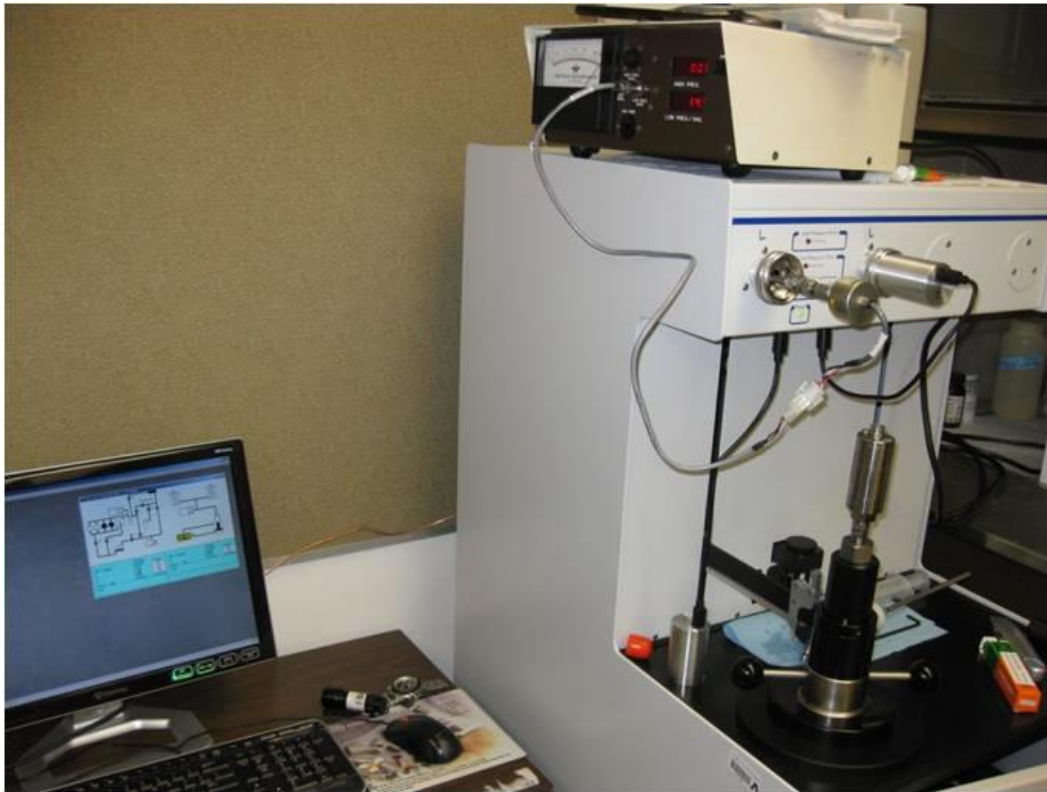
Figure 3-2 MICP apparatus of Micromeritics AutoPore IV 9510.

3.3 Tracer Imbibition

Fluid imbibition is a capillary-force driven process during which a wetting fluid displaces a non-wetting fluid under the influence of capillary suction. In the process of oil/gas recovery from fractured reservoirs, water is spontaneously imbibed from the fracture system into the rock matrix blocks, with the result that oil and gas in the matrix are displaced by the water. Because of the mathematical analogy between diffusion and imbibition, imbibition test can be used to probe a rock's pore connectivity (Hu et al., 2012), and to estimate the crossover length χ (depth to constant accessible porosity) in rocks. In classical homogeneous materials and if gravitational effects are negligible, the distance l to the wetting front increases with the square root of time: $l \sim t^{0.5}$ (Bruce and

Klute, 1956; Philip, 1957; Handy, 1960). If the accessible porosity is uniform with distance, then the cumulative mass of imbibed fluid I behaves identically: $I \sim t^{0.5}$. This relationship gives a slope of 0.5 in log space, which is called the imbibition slope (Hu et al., 2012). Imbibition tests, which are much faster than diffusion tests, involve exposing one face of a rock sample to fluid (for example, *n*-decane), and monitoring the mass uptake over time (e.g., Hu et al., 2001; Schembre and Kovscek, 2006).

Each sample was cut into a rectangular prism with dimensions at about 1.0 cm. All sides except the top and bottom were coated with quick-cure transparent epoxy to avoid evaporation of the imbibing fluid and avoid vapor transport and capillary condensation through the side surfaces of the samples (Figure 3-3). The use of epoxy also allows imbibition up the external surface for us to study 2-D tracer migration. Before being subjected to the imbibition experiments, epoxied samples were oven-dried at 60 °C for at least 48 hours and cooled to room temperature (~23°C) in a desiccator with less than 10% RH to achieve a constant initial water saturation state.

Two fluids (API brine and organic n-decane) with different tracers were used separately in the imbibition experiment. The API brine fluid has affinity for the mineral phase while the organic n-decane fluid has affinity for the kerogen phase. The organic n-decane fluid contains two organic tracers with the elements of rhenium (Re) and iodine (I) while the API brine fluid contains tracers of ReO_4^- (nonsorbing) and Eu^{3+} (sorbing). The tracers in the two fluids (API brine and n-decane) which are readily detected by LA–ICP–MS were used to specifically interrogate the wettability of kerogen and mineral pore spaces and their connectivity.

To measure imbibition rates, the sample was suspended from a bottom-weighing electronic balance and submerged to a depth of about 1 mm in a fluid reservoir as shown in Figure 3-4. The imbibition rate was monitored by automatically recording the sample

weight change over time. The test was conducted for 24 hours on each sample, after

which the sample was removed from the reservoir, momentarily frozen with liquid

nitrogen, freeze-dried at -52 °C and vacuum pulled (about 1 Pa) for a day, and stored at

low relative humidity below 10% prior to LA–ICP–MS analyses. Both the top (tracer-exit)

and bottom (tracer-entry) faces were spot- checked for the presence of tracers, after

which the sample was dry cut transversely in the imbibition direction with a low-speed

diamond saw (Buehler IsoMet). A grid of spot analyses was then performed by LA–ICP–

MS on the saw-opened interior face to map the tracer distribution from imbibition.

A　　　　　**B**　　　　　**C**　　　　　**D**　　　　　**E**
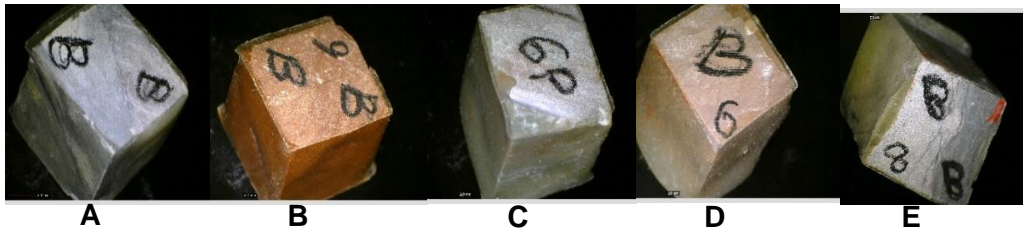
Figure 3-3 Labelled samples (A-E) showing TF1, TF2, TF3, TF4 and TF5 samples

respectively cut into cubes and epoxied.
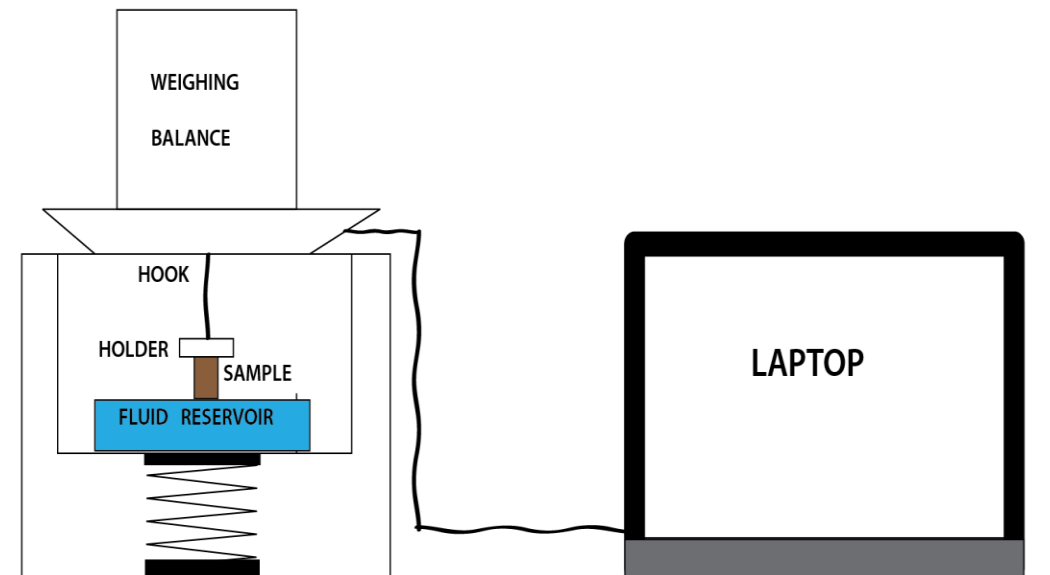
Figure 3-4 Schematic diagram of the apparatus used for the tracer imbibition test.

3.4 Saturated Diffusion

The Saturation diffusion test allows us to study the rate at which the chemical tracers migrate in saturated pore spaces by diffusion. Organic n-decane fluid, with tracers the same as the one used in the tracer imbibition test (described above), was used in the saturation diffusion experiment.

Prior to the saturation diffusion experiment, vacuum saturation test was conducted on the samples. The dried samples were degassed in a sample chamber under 99.99% vacuum, and fully immersed in the saturating fluid without tracers with the aim of fluid occupying the evacuated pore spaces in the samples. Subsequent to immersion, pressurized CO_2 was introduced into the chamber to further drive the fluid into the pores of the samples (Figure 3-5). By weighing the samples prior to and after saturation, the total mass of fluid into the samples was used to calculate the accessible pore volume from vacuum saturation.

To conduct the saturated diffusion test, fully-saturated samples from the vacuum saturation test were placed on a teflon mesh inside a high volume (800 mL) tracer solution reservoir (tracers in n-decane, the saturating fluid of vacuum saturation; Figure 3-6) for 25 hours for tracers to diffuse into the samples such that only the bottom of the sample (to reduce hydraulic head differences) touched the tracer solution, which was constantly stirred with a magnetic stirrer. The reservoir volume was 800 mL, compared to the samples' pore volume of less than 0.05 mL; this high volume ratio ensured a constant tracer concentration (as required to satisfy the boundary condition of the applicable mathematical solution of the diffusion equation). The samples were then removed from the reservoir, frozen with liquid nitrogen, freeze-dried at -52 °C and near-vacuum (about 1 Pa) for a day, and stored at low relative humidity below 10% prior to LA–ICP–MS analyses. Each sample was spot-checked for the presence of tracers at the diffusion-bottom and upper faces.

Figure 3-5 Vacuum saturation apparatus.

Figure 3-6 Saturated diffusion apparatus.

After tracer imbibition and saturated diffusion tests (described above) was performed on the samples, laser ablation coupled with inductively coupled plasma- mass spectrometry (LA-ICP-MS) (Figure 3-7) was used to map the distribution of the tracers and the depth at which the concentration was reached in the samples; both are related to the pore connectivity of the samples.

For the laser ablation system (New Wave; Freemont, CA), we used a 100 μm spot diameter UP-213 laser to vaporize a hole in each sample at sub-micron depth increments; elements entrained in the vapor were analyzed with ICP–MS (PerkinElmer/SCIEX ELAN DRC II; Sheldon, CT). In this way, tracer concentration profiles related to accessible porosity were measured directly, rapidly, and with high sensitivity. The LA–ICP–MS approach made it possible to generate 2-D maps of the tracer distributions in samples at a spatial resolution of microns, and a concentration limit of low-mg/kg (Hu et al., 2002; Peng et al., 2012; Hu and Mao, 2013).

28

In this test, the interior face of the samples was mapped using a two-grid scheme to capture the tracer penetration into the samples. The first grid was used in an area of about 10 mm x 0.3 mm (in the direction of imbibition/diffusion), close to the sample bottom, with a 100 μm laser spot size and 100 μm spacing between spots for the imbibition/diffusion direction. A second grid was then used to the right of the first grid with about 800 um spacing among laser spots for the imbibition/diffusion direction. This close gridding was performed in the area close to the bottom of the sample because the bottom of the sample is usually more concentrated with tracers than the top of the sample.

Figure 3-7 Laser ablation coupled with inductively coupled plasma- mass spectrometry (LA-ICP-MS) apparatus.

Chapter 4

Results and Discussion

4.1 Mercury Injection Capillary Pressure (MICP)

As an imperative method for characterizing rock pore systems, MICP tests were performed on samples from all the members of the Three Forks Formation to obtain their pore-throat size distribution information; the results are shown in Figures 4-1 - 4.3. According the petrophysical work on "Predicting reservoir system quality and performance" by Hartmann and Beaumont (2000), pore sizes are classified as nanopores (<0.1 µm), micropores (0.1-0.5 µm), mesopores (0.5-2.5 µm), macropores (2.5-10 µm) and megapores (>10 µm). The MICP results show that the dominant pore-throat sizes for the Three Forks Formation samples are less than 0.1 µm and therefore fall in the nanopore range.

Table 4-1 MICP Results for the Three Forks Formation Samples

Sample ID	Bulk Density (g/cm^3)	Apparent Density (g/cm^3)	Median Pore-throat Diameter (nm)	Porosity (%)	Permeability (nD)	L_e/L [square root of (tortuosity*porosity)]
TF1	2.92	2.95	269.6	1.16	2585	0.91
TF2	2.54	2.75	8.6	7.92	25.06	7.52
TF3	2.59	2.76	7.9	5.93	13.93	6.85
TF4	2.61	2.77	6.0	5.99	11.19	6.45
TF5	2.72	2.83	35.7	3.82	125.5	3.2

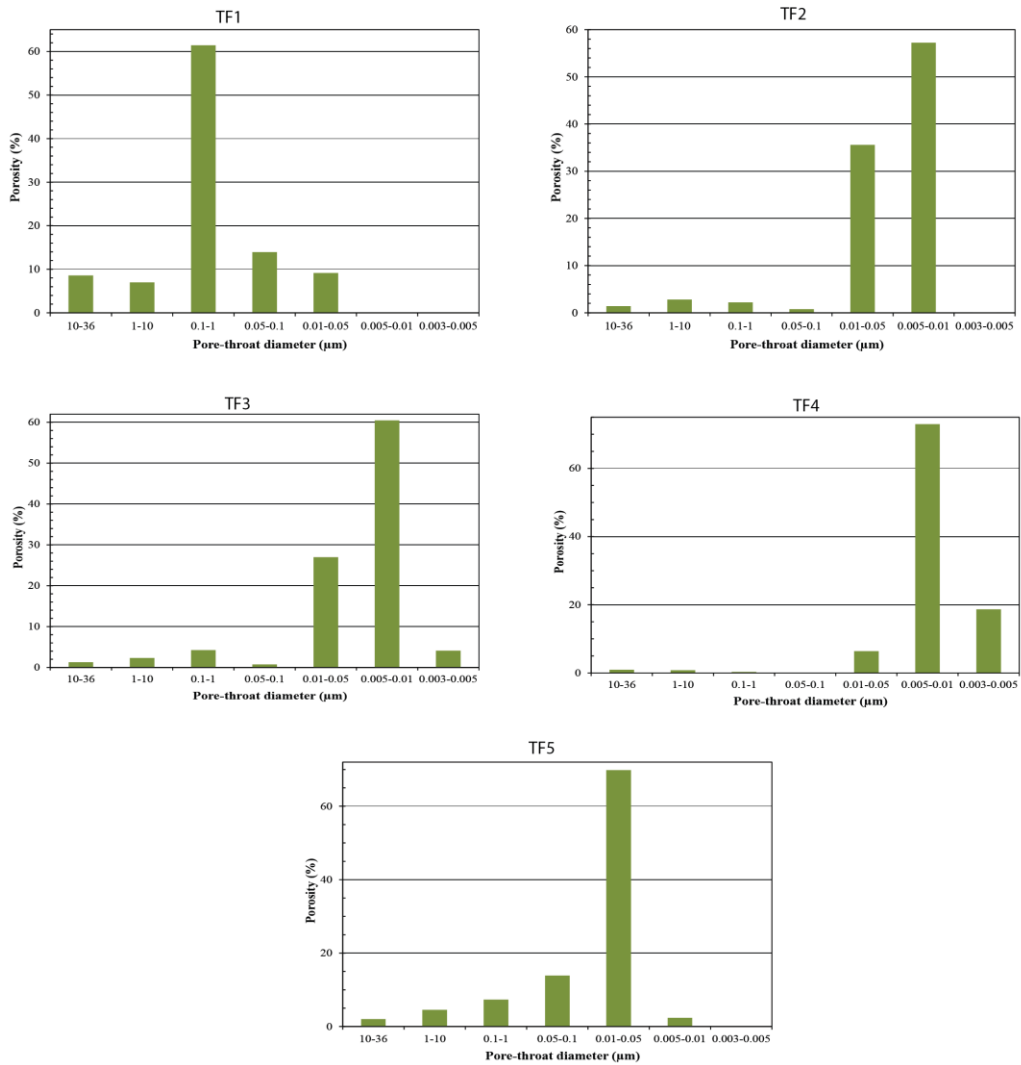Figure 4-1 Comparison of MICP results from all the Three Forks Formation units showing histogram plots of porosity against pore-throat diameter.
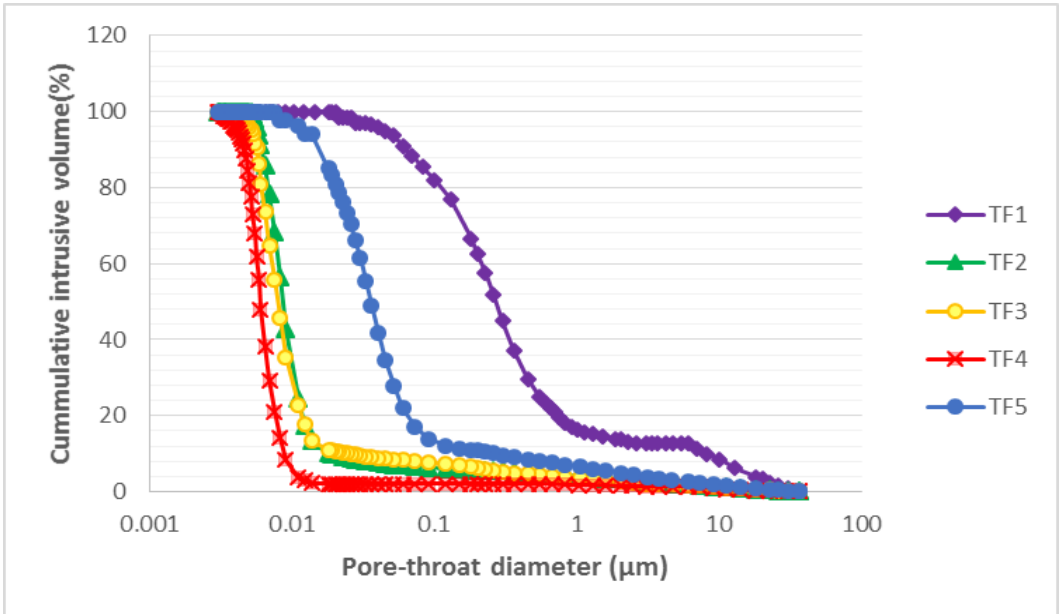
Figure 4-2 Comparison of MICP results from all the Three Forks Formation units showing
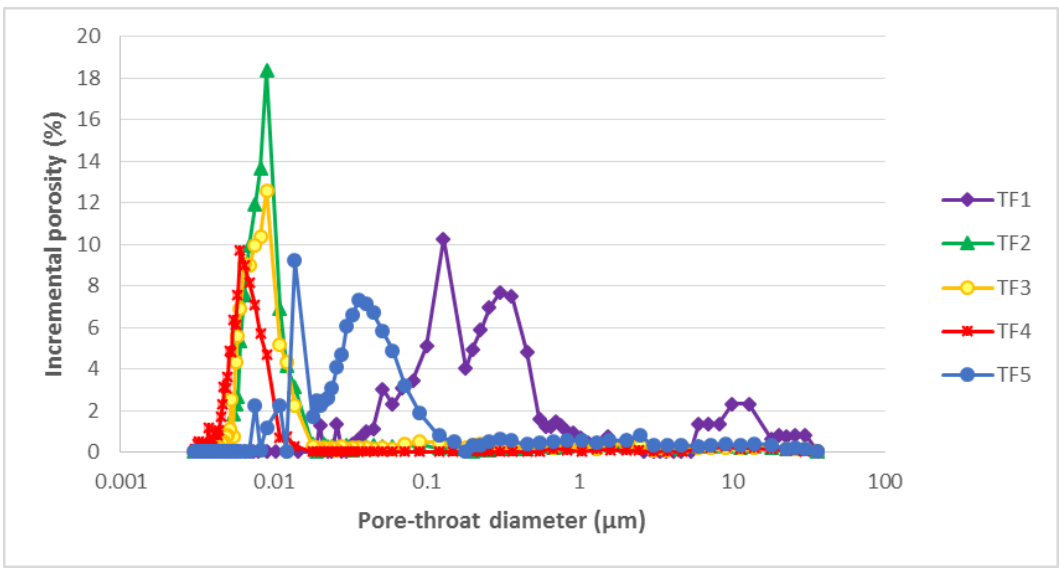
cumulative porosity vs. pore-throat diameter.

Figure 4-3 Comparison of MICP results from all the Three Forks Formation units showing

incremental porosity vs. pore-throat diameter.

The results show that TF1 has the lowest porosity (~1.2%) with more than 60% of the total porosity occupied by larger pores (above 0.1-1 µm). TF5 also has a low porosity (~3.8%) compared to the other members of the formation. In contrast to TFI and TF5, TF2, TF3 and TF4 have high porosities with only a small percentage of their pore spaces occupied by large pores (above 10 µm).

In Figure 4-2, the cumulative intrusion curves of TF1 and TF5 exhibit different behaviors from the other members of the formation. This is consistent in with Figure 4-3 and Table 4-1, in which the median pore-throat diameter of TFI and TF5 are larger than TF2, TF3 and TF4. This difference probably reflects the heterogeneity of the Three Forks Formation. The Y-axis of "Cumulative Intrusion Volume" for Figures 4.3 and 4.4 is arbitrarily set to be 100% for the minimum measureable pore-throat of 3 nm, dictated by the maximum intrusion pressure of our MICP instrument; there may be some non-negligible pore volume accessible only through pore-throats <3 nm. However, the volume of pores accessible via pore-throats <3 nm is not expected to be large, or to play an important role in fluid migration. The MICP results show that the pores (about 60–80% by volume) in all five members of the Three Forks formation are dominantly smaller than 10 µm.

Tortuosity which is also derived from MICP data is another parameter that can be used to evaluate pore systems. Tortuosity is defined as the ratio of the actual distance traveled between two points to the minimum distance between the two points. It characterizes the convoluted pathways of fluid flow through rock systems. Following Gommes et al.'s (2009) approach of relating geometrical tortuosity to the travel paths that molecules travel through porous medium, the L_e/L ratios within the Three Forks Formation are also presented in Table 4-1. The results show relatively large values of tortuosity which implies that fluid particles will need to make way through some tortuous

33

pathways in order to migrate from one location to another within the Three Forks Formation. For example, a tortuosity of 7.52 in TF2 means that it will take about 7.52 centimeters for a fluid particle in that Unit to travel a linear distance of one centimeter in the formation. The results in Table 4-1 show that TF2 has the most tortuous pathways followed by TF3, TF4 and TF5 respectively. Based on the results obtained we believe that the nanopores of the Three Forks Formation are poorly connected and fluid particles will require lots of time to connect pathways of limited distance. It should also be noted that not all of the pathways in the samples have the same length. Some lengths may be shorter or longer than the average lengths, hence, compositionally different members may have a large fraction of similar lengths.

4.2 Tracer Imbibition

Spontaneous fluid (API brine or n-decane) imbibition into hydrocarbon-saturated rocks is an important physical process during water injection into petroleum and geothermal reservoirs. Both cumulative imbibition height and imbibition time were plotted in log-log scales for all the Three Forks formation samples. During the initial thirty seconds or so of each imbibition experiment, it was observed that the samples were not stable and vibrated slightly in the vertical direction from touching the fluid. Additionally, the influences of the buoyancy caused by inserting the sample into the fluid also caused instability and inaccurate results at the very beginning of the experiment. For times after this initial period of instability, a linear relationship was observed in the logarithmic plots of cumulative imbibition height versus imbibition time. There might also be some error although the effect of buoyancy on the data was calibrated by weighing the sample after the fluid imbibition test.

Table 4-2 Imbibition test results for the Three Forks Formation samples

Sample ID	Fluid	Length (cm)	Width (cm)	Height (cm)	Slope
TF1	API brine	1.135	1.099	1.044	0.424 → 0.129
TF2	API brine	0.992	1.017	0.958	0.709 → 0.272
	n-decane	1.114	0.95	1.012	0.592
TF3	API brine	1.06	1.051	0.994	1.179 → 0.292
TF4	API brine	1.05	0.964	0.983	0.491 → 0.256
	n-decane	1.016	1.058	1.073	0.223
TF5	n-decane	1.004	0.986	1.088	0.200

The relationship between the fluid gain and the imbibition time in the sample is shown in Figures 4-4 and 4-5. Linear correlations are observed between the amount of fluid imbibed and the imbibition time when plotted in log-log space (Hu et al., 2012). However it is also observed that the line does not go through the origin, as expected; this phenomenon may be brought about by the influence of gravity. The imbibition experiments produced a range of imbibition slopes from 0.129 to 1.179 (Table 4-2). A gradual slope change is observed from higher slope values to lower slope values across all the samples, which is indicative of poorly connected pores (Figures 4-4 and 4-5; Table 4-2). The larger slope values were probably due to initial sample settling, combined with the short time needed for the wetting front to reach the sample top; this gave relatively few data points to calculate the imbibition slope.

The results also show that although the TF3 and TF4 samples have similar porosity and permeability values, TF4 sample consistently exhibited a lower imbibition slope (Table 4-2), indicating a poor pore connectivity than the TF3 sample. Poorly connected pores were also evident in the other members of the formation: these samples also have low porosity and nanometer-sized pores, which tend to be associated with low pore connectivity. For the TF2 and TF3 samples, imbibition slopes varied between 0.26 and 1.18, exhibiting intermediate pore connectivity. The sample shape may also have some influence on the slope values, as reported by Hu et al. (2012), tall thin samples (with intermediate pore connectivity) are more likely to exhibit the 0.26 imbibition slope, perhaps later crossing over to 0.5-type behavior, while short, squat samples were more likely to have a slope of 0.5. With a sample shape factor of ~1.0, TF4 imbibition proceeded as a classical-type (0.491), and then switched to an anomalous (0.256) behavior. This change in slope behavior from classical to anomalous is also observed in samples TF1, TF2, TF3 and TF5. The distance to the wetting front at which the slope changed is known as the crossover length χ of percolation theory.

According to the percolation theory (the study of how pore connections affect the resultant macroscopic properties), an imbibition slope of 0.5 indicates well pore connectivity and a slope of ~0.26 with connectivity barely above p_c, which is the percolation threshold. At intermediate values (of about, $p \approx 0.25$), the slope transitions from 0.26 to 0.5 after some finite imbibition time. In other words, just above the percolation threshold, fluid imbibition (analogous to solute diffusion) behaves somewhat "classical" (Fickian) at short times and distances, but later assumes anomalous long-term behavior. Consistent with percolation theory and pore-scale network modeling, this work on the different rock units of the Three Forks formation shows that anomalous behavior (slope of <0.26) is dominantly observed at some scales in all the samples.

The slope of n-decane imbibition for TF2 is 0.592 which is much higher than 0.272 for API brine imbibition, this indicates an oil-wet property of the TF2 samples. This observation was made in the rest of the samples. Another important characteristic observed was that the n-decane fluid was more readily imbibed by the samples in the initial phase of the experiment than the API fluid. During the imbibition period, n-decane fluid may have been able to enter the pore space in sufficient quantity to reach the sample top in a shorter time than the API brine fluid. This observation also means that the rock has poor pore connectivity to API brine but good pore connectivity to n-decane.
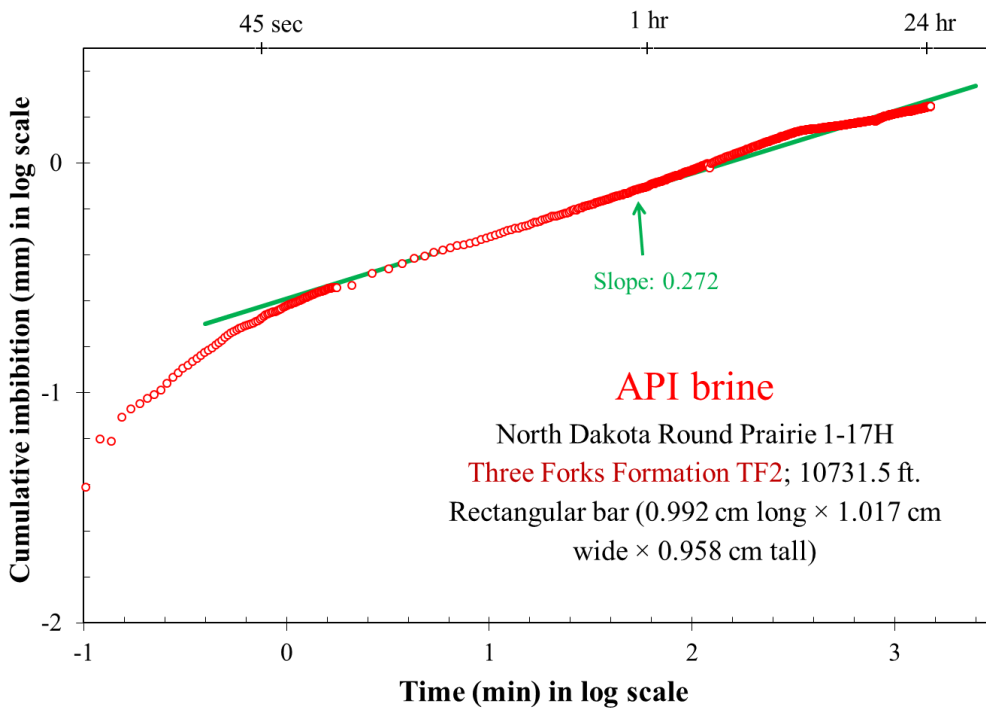

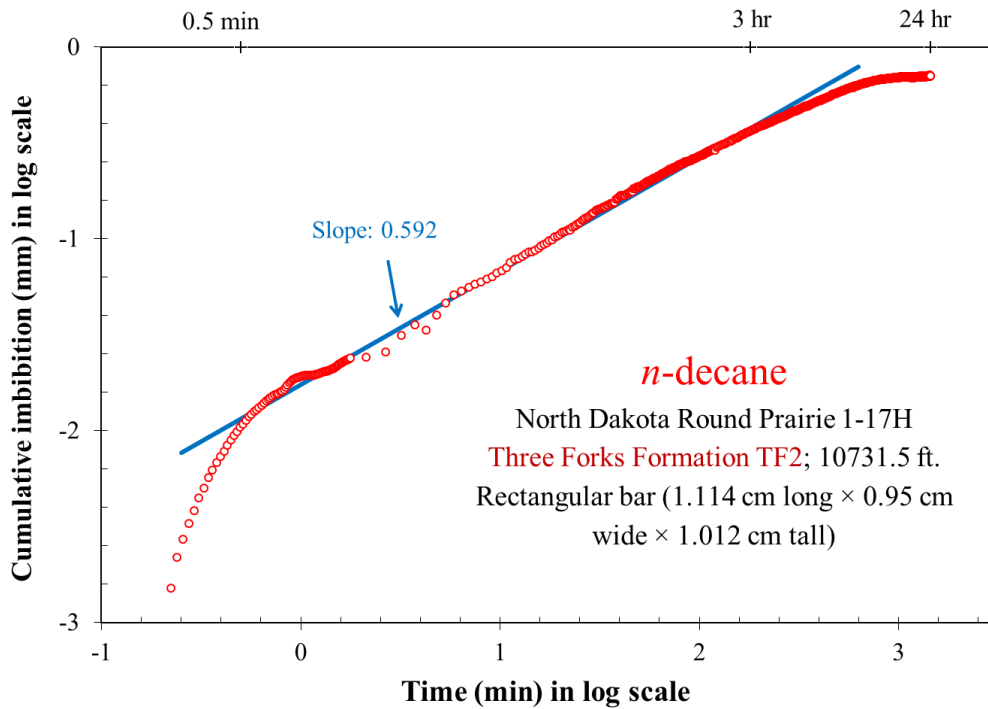Figure 4-4 Imbibition results plot for TF2 sample using API brine fluid.

Figure 4-5 Imbibition results plot for TF2 sample using n-decane fluid.

Results for API brine tracer imbibition into the Three Forks Formation samples are shown in Figures 4-6 to 4-8. Distribution of both API brine tracer is very heterogeneous. The steep decline of tracer concentration observed over a distance of about 100 μm from the sample edge also indicates poor pore connectivity in the Three Forks Formation samples. The white portions observed on the map implies no tracer penetration in the pores as a result very tight pore throats while the red zones indicate regions of high tracer concentrations. Although the tracer concentration occurs in a sporadic manner, high concentrations are dominantly seen along the walls of the samples. The results show that rhenium (ReO_4^-) tracers migrated through the nanopores of the samples farther than the europium Eu^{3+} tracers, probably due to their smaller molecular size. The bottom part of the samples are observed to have higher

concentrations of the tracers especially (ReO$_4$-) tracers which is also probably because that part of the sample makes the closest contact with the imbibing fluid as it is submerged in it.

Additionally, it is observed that the non-sorbing rhenium tracers (ReO$_4$-) occupied the pore spaces and did not interact with the sample matrix which indicates edge-accessible porosity distribution within the samples. The decrease of tracer concentration observed with depth also indicates poorly-connected pore spaces within the samples.
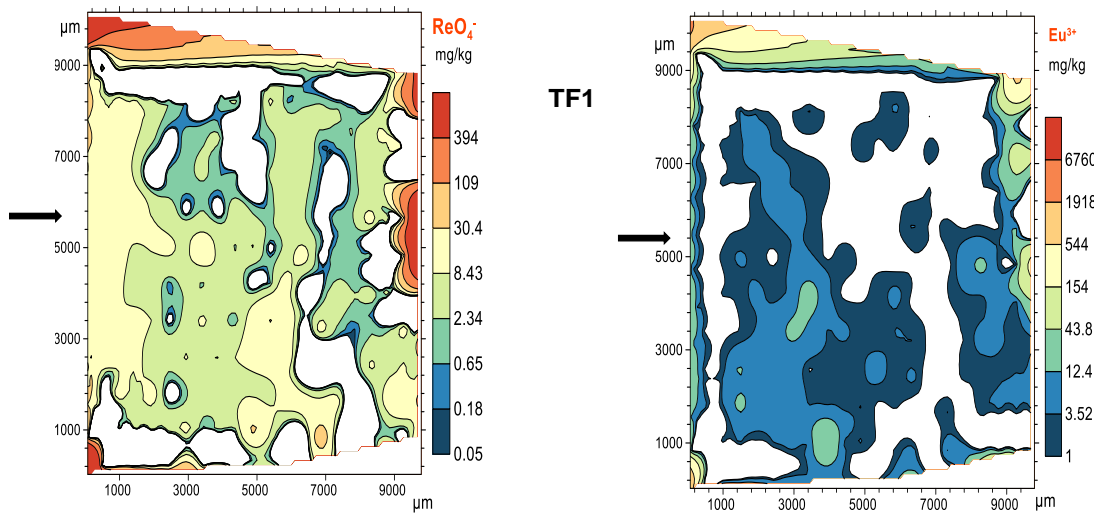

Figure 4-6 Tracer imbibition results for Round Prairie TF1 samples (Interior face) using API brine fluid with tracers of perrhenate and europium ions. Arrow on the left indicate the base of sample and direction of tracers' imbibition.
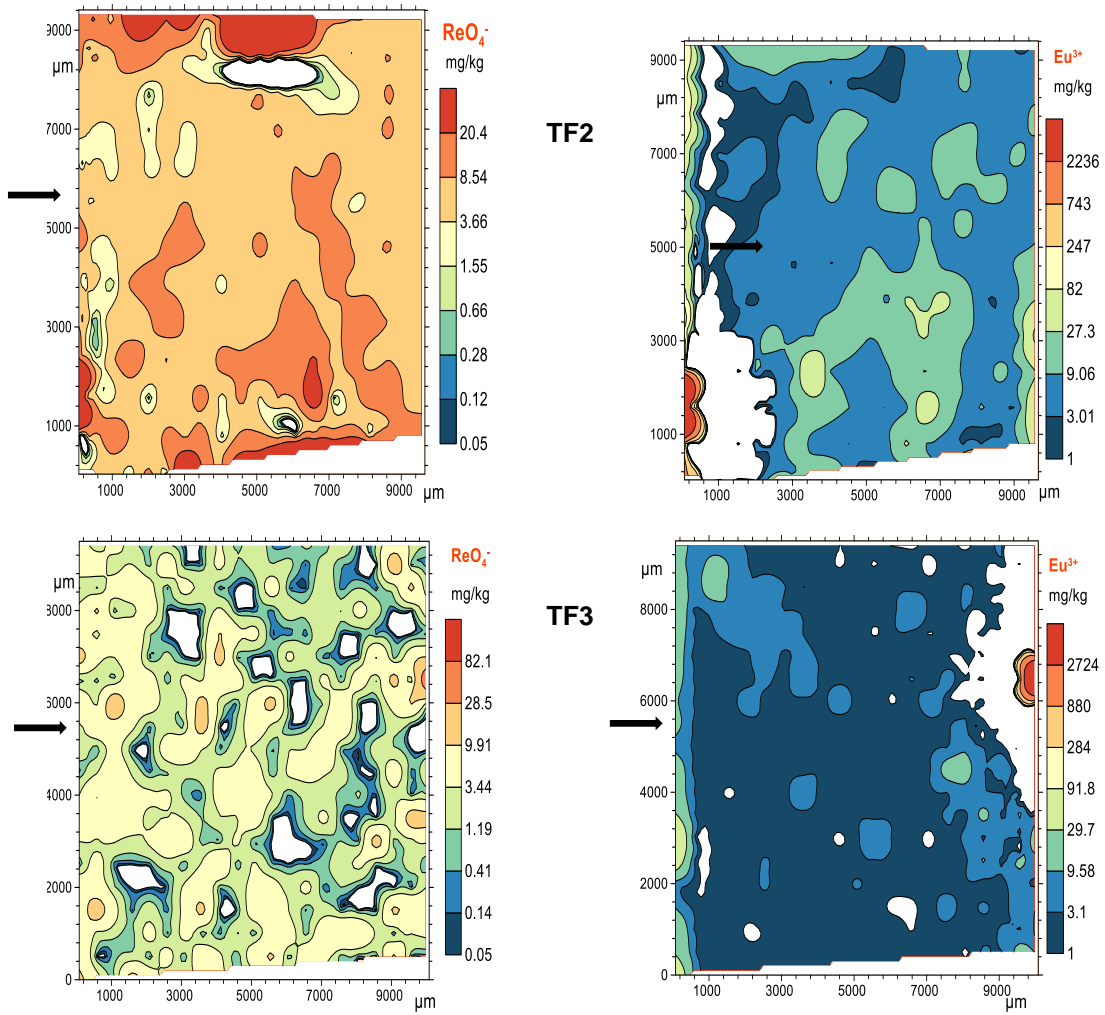
Figure 4-7 Tracer imbibition results for Round Prairie TF2 and TF3 samples (Interior face)
using API brine fluid with tracers of perrhenate and europium ions.
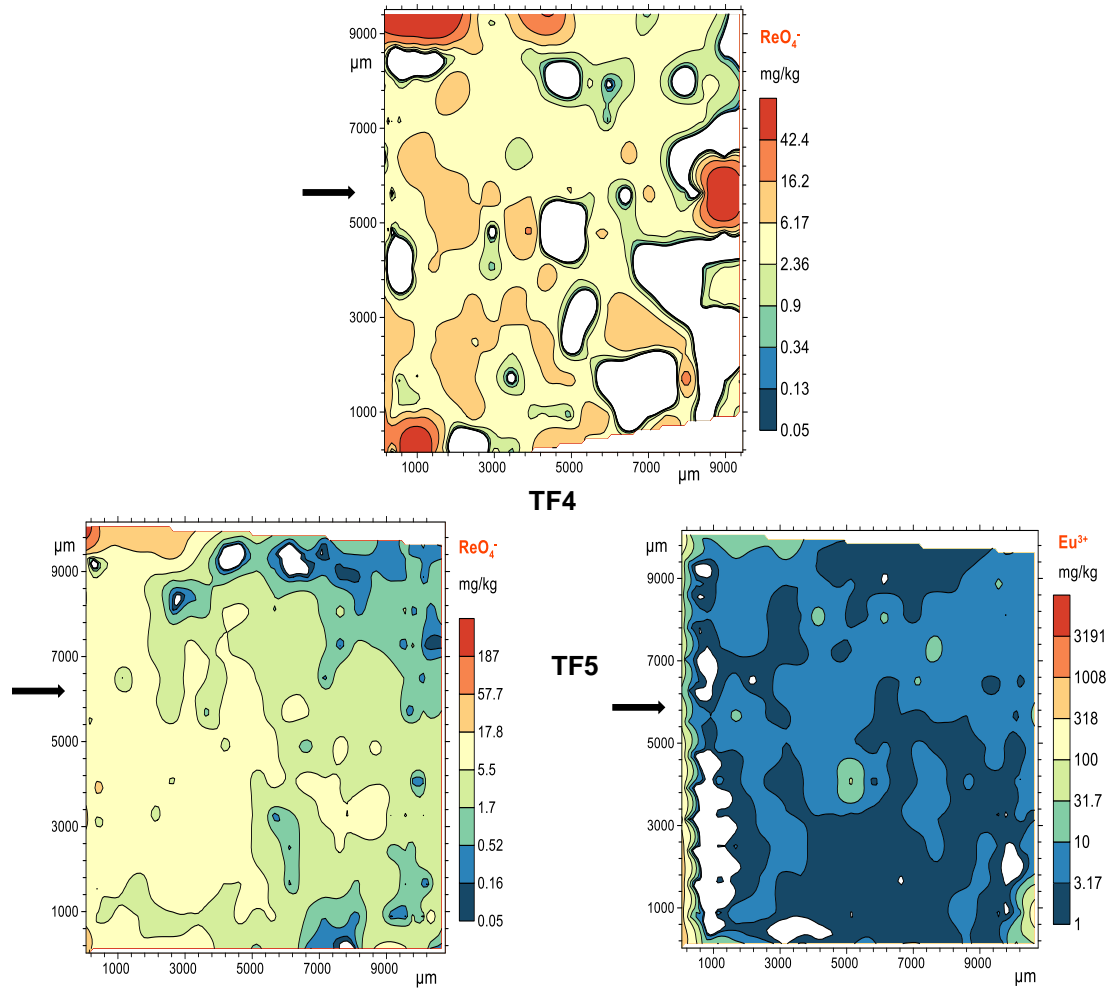
Figure 4-8 Tracer imbibition results for Round Prairie TF4 and TF5 samples (Interior face) using API brine fluid with tracers of perrhenate and europium ions.

Results for n-decane tracer imbibition into the Three Forks Formation samples are also shown in Figures 4-9 to 4-11. Distribution of organic fluid based tracer is very heterogeneous and in a similar pattern as that of the API brine imbibition test. Although the tracer concentration occurs in a sporadic manner, high concentrations are dominantly seen along the walls of the samples. It is also observed that the iodine tracer penetrated the samples more than the rhenium tracer (ReO_4-) which is probably due to the smaller

41

molecular size of the iodine tracers. Additionally, the high concentration of iodine from the bottom of the sample through the side and along the top of the sample suggests that migration of the tracer through the sample's exterior surface was faster than migration through the tortuous pathways within the sample.

Samples TF2, TF3 and TF4 show the most red zones almost (high tracer concentration) throughout the sample surface while samples TF1 and TF5 show the least concentration of the tracers. This implies that samples TF2, TF3 and TF4 have more nanometer size kerogen in the nanopores that are connected. Experimental results from MICP tests consistently indicate poor pore connectivity of the Three Forks Formation samples. The practical implication is that the migration of hydrocarbon from rock matrix to fracture in well bore is expected to be slow and will affect the hydrocarbon recovery.
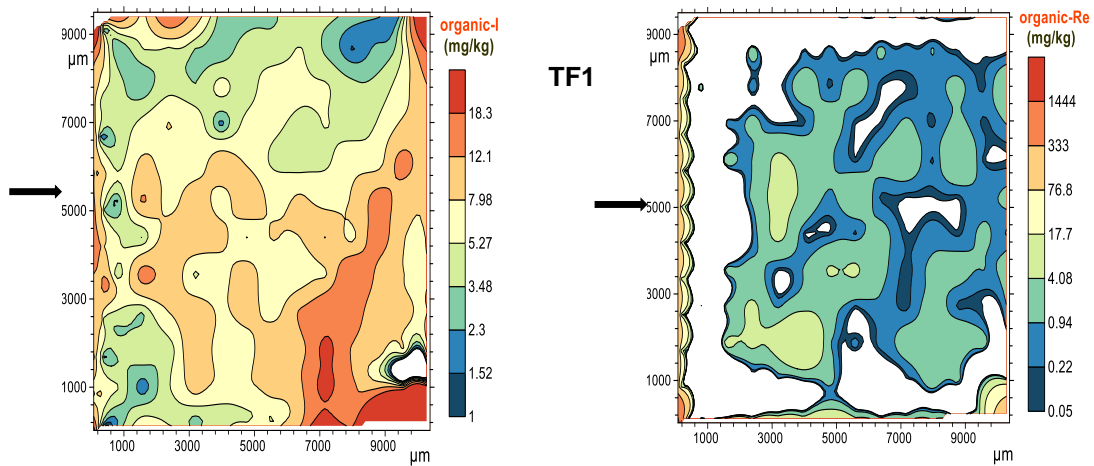
Figure 4-9 Tracer imbibition results for Round Prairie TF1 samples (Interior face) using n-decane fluid with two organic tracers'. Arrow on the left indicate the base of sample and direction of tracers' imbibition.

Figure 4-10 Tracer imbibition results for Round Prairie TF2 and TF3 samples (Interior face) using n-decane fluid with two organic tracers.

Figure 4-11 Tracer imbibition results for Round Prairie TF4 and TF5 samples (Interior face) using n-decane fluid with organic tracers.

4.3 Saturated Diffusion

Rock matrix diffusion is an important transport process in geologic materials of low permeability. For predicting the fate and transport of hydrocarbons, a detailed understanding of the distribution and migration of hydrocarbons by diffusion processes in

natural porous media is essential. In this study, diffusive tracer transport was investigated in the Three Forks Formation.

Two-dimensional elemental mapping for the tracers was conducted for the interior face (Figures 4-12 to 4-14). The 2-D side wall diffusion is much quicker than the 2-D interior diffusion, with the concentration of tracers differing in several orders of magnitude. The results indicate that only about 0.1% to 1% of the porosity in the middle of a sample is connected to the exterior which consistent with a percolation theory interpretation of pore connectivity. For two molecular tracers in n-decane with the sizes of 1.393 nm×0.287 nm×0.178 nm for 1-iododecane and 1.273 nm×0.919 nm×0.785 nm for trichlorooxobis (triphenylphosphine) rhenium, much less diffusive penetration was observed for wider molecules of trichlorooxobis (triphenylphosphine) rhenium in oil-wetting samples with median pore-sizes of several nanometers; the results indicates the entangling of nano-sized molecules in nanopore spaces of samples. This means that only a very small portion of the nanopores in the Three Forks Formation samples are connected to the sample surface for diffusion. The practical implication is that the out-diffusion of hydrocarbon is also expected to be slow, of limited quantity, and largely from rock matrix that is within some small distance from a fracture; this will affect the hydrocarbon recovery in stimulated shale reservoirs. Additionally, it should be noted that such results are obtained under atmospheric pressure; under reservoir pressure conditions however, the distance of connected nanopores from the sample edge will be somewhat larger.

Figure 4-12 Saturated diffusion results for Round Prairie TF1 and TF2 samples (Interior face) using n-decane fluid with tracers of iodine and rhenium. Arrow on the left indicate the base of sample and direction of tracers' diffusion.
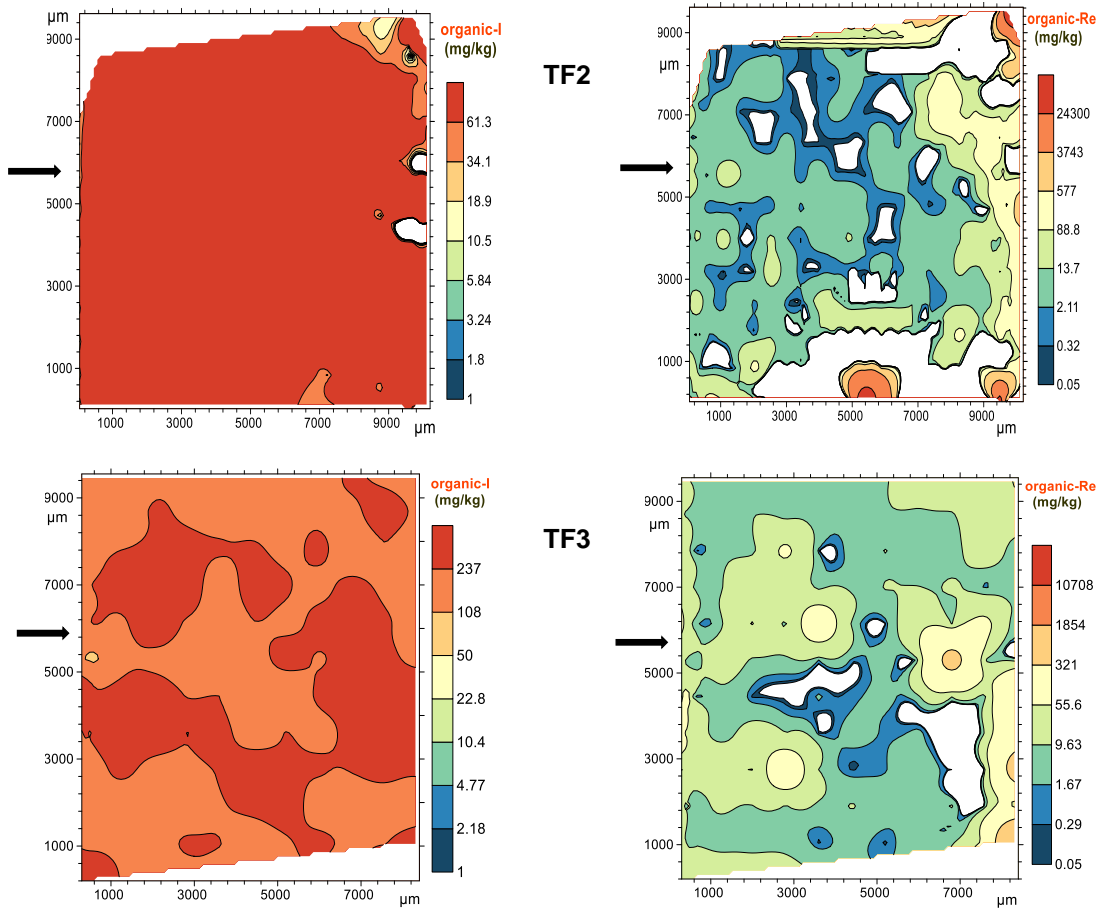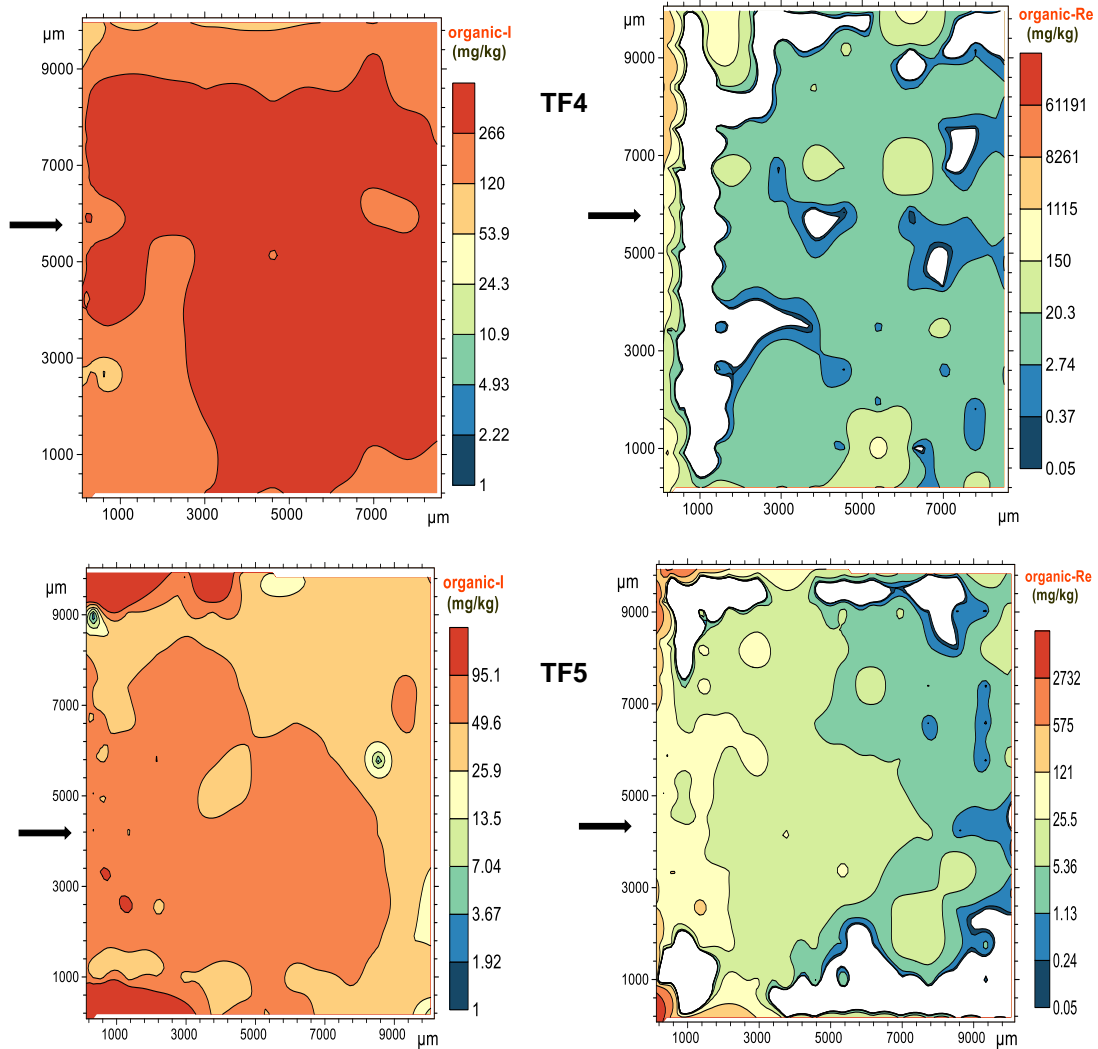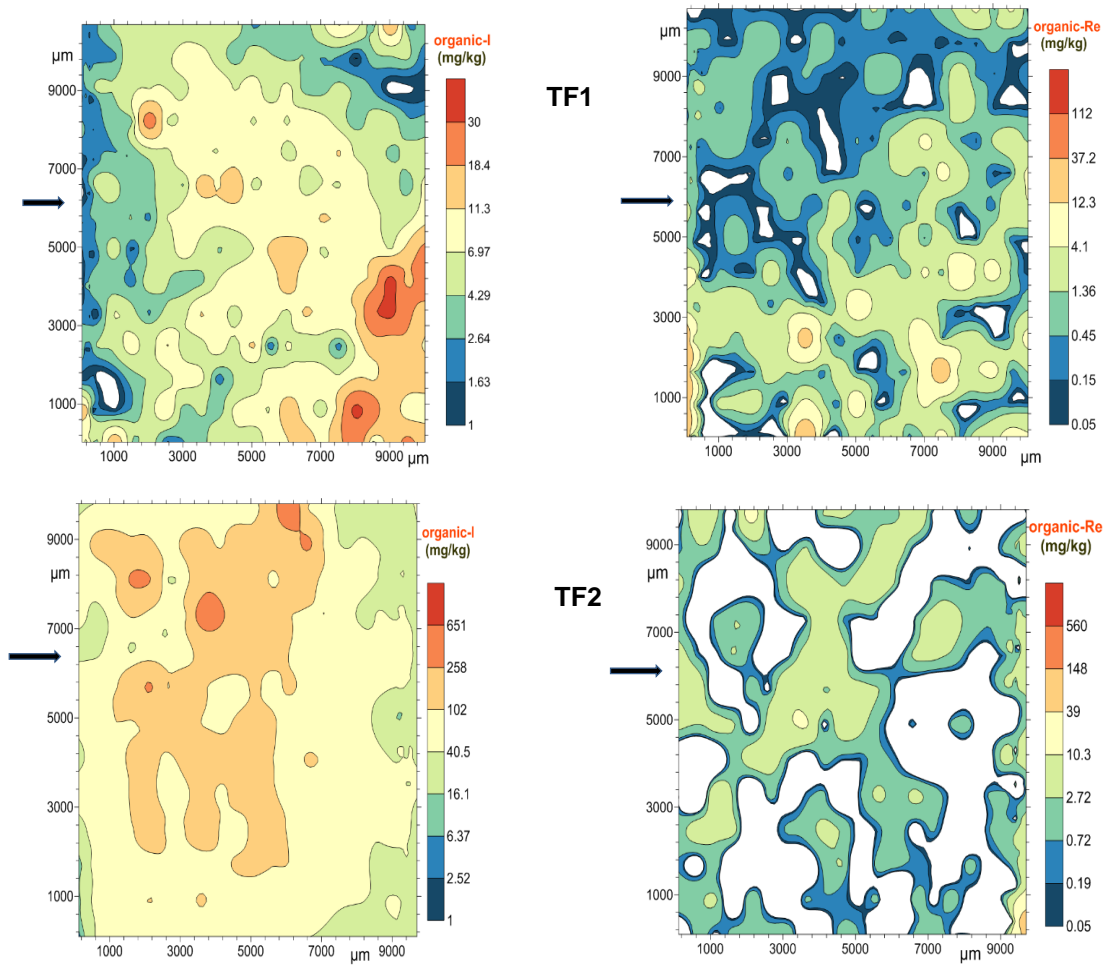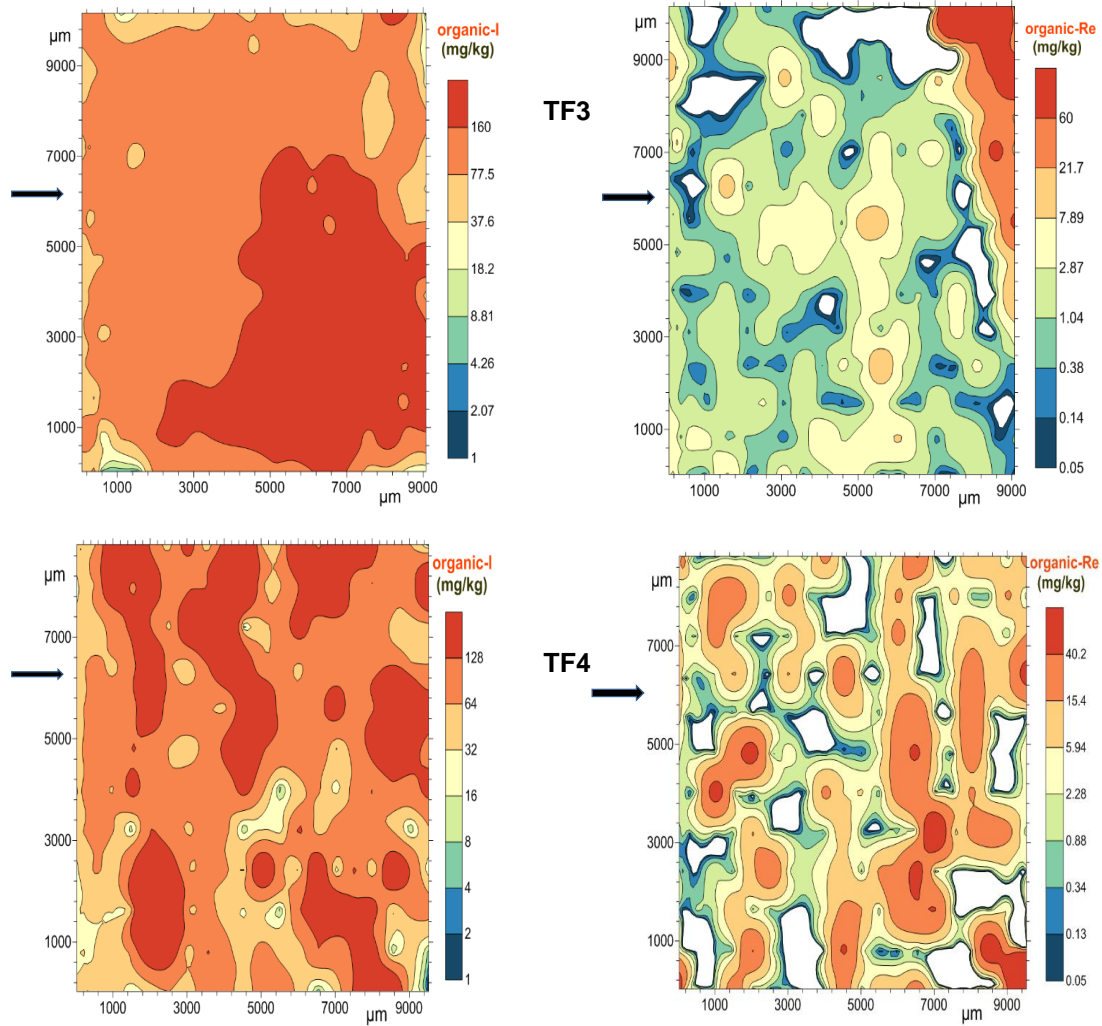
46

Figure 4-13 Saturated diffusion results for Round Prairie TF3 and TF4 samples (Interior face) using n-decane fluid with tracers of iodine and rhenium.
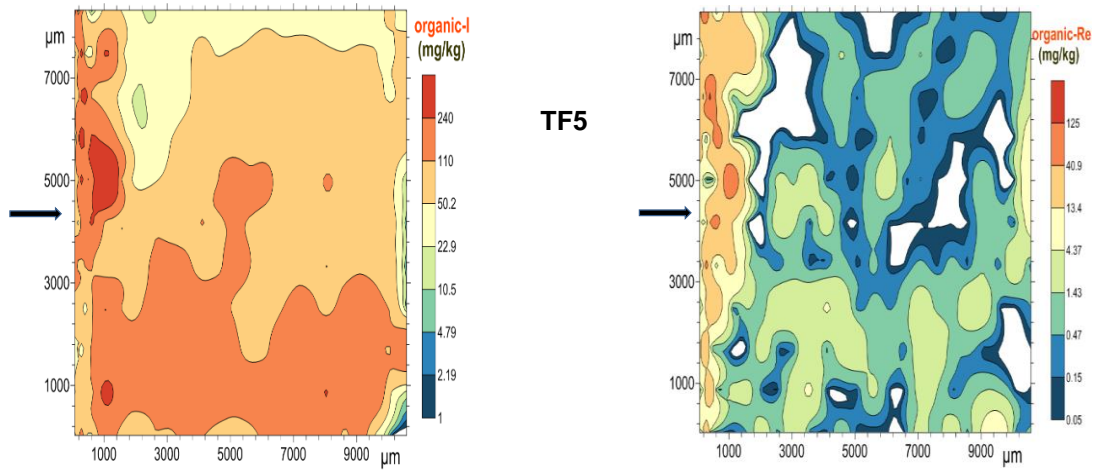
Figure 4-14 Saturated diffusion results for Round Prairie TF5 samples (Interior face)

using n-decane fluid with tracers of iodine and rhenium.

Chapter 5

Conclusion and Recommendation

5.1 Conclusions

The main goal of this work was to improve fundamental understanding of fracture–matrix interaction and its implications in hydrocarbon recovery in the Three Forks Formation samples. This process–level understanding enables economic and sustainable production from unconventional reservoirs. The focus on pore structure (geometry and connectivity) in this work in particular could have a major impact on hydrocarbon production from shale resources, because steep production decline and low recovery has been plaguing the oil and gas industry.

We used multiple approaches to investigating pore structure, and the resulting anomalous fluid migration, in the Three Forks Formation samples. These experimental approaches include mercury injection capillary pressure, tracer imbibition and saturated diffusion followed by LA–ICP–MS mapping. Results show that the Three Forks Formation samples pores are predominantly in the nm size range, with a measured median pore-throat diameter of about 615.4, 8.6, 7.9, 6 and 35.7 nm for Units TF1, TF2, TF3, TF4 and TF5 respectively.

The nanometer pore size, low permeability values and poor pore connectivity lead to extremely low diffusion rates in sample matrix, as measured using saturated diffusion approach and laser ablation–ICP–MS mapping.

Additionally, results show that connected matrix pores in samples seem to be limited to a few mm from the sample edge, followed with a sporadic and sparse connection deeper into the sample. This poor pore connectivity and limited connected distance into sample matrix from sample edge (i.e., fracture) will lead to low recovery and

low overall production. The poor pore connectivity of the Three Forks Formation samples, probably associated with low porosities and nanopores, was also indicated by the anomalous slope behavior (around 0.28) obtained from imbibition tests suggested by the percolation theory and the high tortuosity values derived from MICP data.

The overall outcome of this work bridges the knowledge gap regarding the effects of pore connectivity on diffusion-limited gas transport, as well as low overall hydrocarbon production observed in hydraulic-fractured shale reservoirs.

5.2 Recommendations

Although the results of this work helps bridge the knowledge between pore connectivity and hydrocarbon production, a more detailed work should be conducted into studying fluid flow within the nanopores of tight rocks. Additional work should be done on different wells from different parts across the formation as this will help better understand the dynamics of the fluid flow in the rocks on a larger scale. Other innovative approaches such as Nuclear Magnetic Resonance (NMR), N2 adsorption isotherm and hysteresis, and Small Angle Neutron Scattering (SANS) analyses should be employed to further understand the migration of hydrocarbon molecules from the tight rock matrix into the induced fracture in unconventional systems.

References

Anna, L., Pollastro, R. & Gaswirth, S., 2011. Williston Basin Province- Stratigraphic and Structural framework to a geologic assessment of undiscovered oil and gas resources, Chap 2 of. f U.S. *Geological Survey Williston Basin Province Assessment team, Assessment of undiscovered oil and gas resources of the Williston Basin Province of North Dakota, Montana, and South Dakota, 2010, Volume U.S. Geological Survey Digital Data Series* 69-W, p. 17.

Akin, S., J.M. Schembre, S.K. Bhat, and A.R. Kovscek. 2000. Spontaneous imbibition characteristics of diatomite. *J. Petrol. Sci. Eng.,* 25: 149–165.

Babadagli, T. and C.U. Hatiboglu. 2007. Analysis of counter-current gas–water capillary imbibition transfer at different temperatures. *J. Petrol. Sci. Eng.,* 55 (3–4): 277–293.

Boving, T.B. and P. Grathwohl. 2001. Tracer diffusion coefficients in sedimentary rocks: correlation to porosity and hydraulic conductivity. *J. Contam. Hydrol.,* 53(1–2): 85–100.

Carniglia, S.C. 1986. Construction of the tortuosity factor from porosimetry. *J. Catal.*, 102: 401–418.

Chaudhary, A.S., C. Ehlig-Economides, and R. Wattenbarger. 2011. Shale oil production performance from a stimulated reservoir volume. *SPE Annual Technical Conference and Exhibition, Denver, CO, USA, 30 Oct. – 2 Nov., 2011.* SPE 147596.

Chilingar, G.V., R. Main, and A. Sinnokrot. 1963. Relationship between porosity, permeability, and surface areas of sediments. *J. Sediment. Petrol.,* 33(3): 759–765.

Cui, X., A. Bustin, and R. Bustin. 2009. Measurements of gas permeability and diffusivity of tight reservoir rocks: Different approaches and their applications. *Geofluids,* 9: 208–223.

Cunningham, R.E. and R.J.J. Williams. 1980. Diffusion in gases and porous media, *Plenum, New York.*

Christopher, J. E., 1961. Transitional Devonian - Mississippian Formations of southern Saskatchewan: Saskatchewan Mineral Resources Report 66, Regina, Saskatchewan, 103 p.

Clarkson, C. R., M. Freeman, L. He, M. Agamalian, Y. B. Melnichenko, M. Mastalerz, R. M. Bustin, A. P. Radlinski and T. P. Blach. 2012. Characterization of tight gas reservoir pore structure using USANS/SANS and gas adsorption analysis. *Fuel,* 95(1): 371-385.

Curtis, J.B. 2002. Fractured shale-gas systems. *AAPG Bull.*, 86(11): 1921-1938.

Curtis, M.E., C.H. Sondergeld, R.J. Ambrose and C.S. Rai. 2012. Microstructural investigation of gas shales in two and three dimensions using nanometer-scale resolution imaging. *AAPG Bull.,* 96(4): 665-677.

Dullien, F.A.L., 1992. Porous Media: Fluid Transport and Pore Structure (2nd Ed.). *Academic Press, San Diego.*

Gao, Z. and Q. Hu. 2012. Using spontaneous water imbibition to measure building materials' effective permeability. *Spec. Topics Rev. in Porous Media- An Intern. J.*, 3(3): 209–213.

Gao, Z. and Q. Hu. 2013. Estimating permeability using median pore-throat radius obtained from mercury intrusion porosimetry. *J. Geophys. Eng.*, 10(2), 025014.

Gommes, C.J., A.J. Bons, Blacher, J. Dunsmuir, and A. Tsou (.2009.) Practical methods
for measuring the tortuosity of porous materials from binary or gray-tone
tomographic reconstructions. *Amer. Inst. Chem. Eng. J.*, 55: 2000–2012.

Grathwohl, P. 1998. Diffusion in Natural Porous Media: Contaminant Transport,
Sorption/Desorption and Dissolution Kinetics. *Kluwer Academic Publishing,
Boston*, pp. 224.

Gerhard, l. C., S. B. Anderson, and D. W. Fischer, 1990, Petroleum geology of the
Williston Basin: AAPG Memoir, v. 51, p. 507-559.

Gerhard, l. C., S. B. Anderson, and J. A. LeFever, 1987, Structural history of the Nesson
anticline, North Dakota, in M. W. Longman, ed., Williston Basin: anatomy of a
cratonic oil province, Denver, Colorado, Rocky Mountain Association of
Geologists, p.337-3S4.

Gerhard, l. C., S. B. Anderson, J. A. LeFever, and C. G. Carlson, 1982, Geological
development, origin, and energy mineral resources of Williston Basin, North
Dakota: *AAPG Bulletin*, v. 66, no.8, p. 989-1020.

Giesche, H., 2006. Mercury porosimetry: a general (practical) overview. *Part. Syst.
Charact.,* pp. 1-11.

GRI (Gas Research Institute). 1996. Development of laboratory and petrophysical
techniques for evaluating shale reservoirs. *Final Report GRI-95/0496*, April 1996

Hartmann, D.J. and E.A. Beaumont. 1999. Predicting reservoir system quality and
performance. In: Beaumont, E.A., Foster, N.H. (Eds.), Exploring for Oil and Gas
Traps: AAPG Treatise of Petroleum Geology: *Handbook of Petroleum Geology*.
p. 9-1–9-154.

Hu, Q., T.J. Kneafsey, R.C. Trautz, and J.S.Y. Wang. 2002. Tracer Penetration into
Welded Tuff Matrix from Flowing Fractures. *Vadose Zone J.*, 1: 102–112.

Hu, Q.H., and X.L. Mao. 2012. Applications of laser ablation☐inductively coupled
plasma☐mass Spectrometry in studying chemical diffusion, sorption, and
transport in natural rock. *Geochem. J.,* 46 (5):459–475.

Hu, Q.H., X.B. Gao, Z.Y. Gao, R.P. Ewing, S. Dultz,and J. Kaufmann, 2014 Pore
Accessibility and Connectivity of Mineral and Kerogen Phases in Shales.
Unconventional Resources Technology Conference (URTeC)

Hunt, A.G., R.P. Ewing, and B. Ghanbarian. 2014. Percolation Theory for Flow in Porous
Media 3rd ed., *Lect. Notes Phys. 880*, Springer, Heidelberg.

Katz, A.J., and A.H. Thompson. 1986. A quantitative prediction of permeability in porous
rock. *Phys. Rev. B 34, pp.* 8179-8181.

Katz, A.J. and A.H. Thompson. 1987. Prediction of rock electrical conductivity from
mercury injection measurements. *J. Geophys. Res.92*, pp. 599-607.

Li, K. 2007. Scaling of spontaneous imbibition data with wettability included. *J. Contam.
Hydrol.*, 89: 218–230.

Li, K. and R.N. Horne. 2001. Characterization of spontaneous water imbibition into gas-
saturated rocks. *SPE J*, 6 (4): 375-384.

Loucks, R.G., R.M. Reed, S.C. Ruppel and D.M. Jarvie. 2009. Morphology, genesis, and
distribution of nanometer-scale pores in siliceous mudstones of the Mississippian
Barnett Shale. *J. Sed. Res.,* 79(11-12): 848-861.

Loucks, R.G., R.M. Reed, S.C. Ruppel and U. Hammes. 2012. Spectrum of pore types
and networks in mudrocks and a descriptive classification for matrix-related
mudrock pores. *AAPG Bull.*, 96(6): 1071-1098.

Ma, S., N.R. Morrow, and X. Zhang. 1997. Generalized scaling of spontaneous imbibition
data for strongly water-wet systems. *J. Petrol. Sci. Eng.,* 18: 165–178.

Makhanov, K., H. Dehghanpour, and E. Kuru. 2012. An experimental study of

    spontaneous imbibition in Horn River shales. *SPE Canadian Unconventional*

    Resources Conference, October 30 - November 1, Calgary, Alberta, Canada,

    DOI 10.2118/162650-MS.

Mehmani, A., A. Token-Lawal, and M. Prodanović. 2011. The effect of microporosity on

    transport properties in tight reservoirs. *Paper SPE 144384 presented at the North*

    American Unconventional Gas Conference and Exhibition, Woodlands, Texas,

    14–16 June. DOI: 10.2118/144384-MS.

Nicolas, M.P.B. 2012. Stratigraphy and regional geology of the Late Devonian-Early

    Mississippian Three Forks Group, southwestern Manitoba (NTS 62F, parts of

    62G, K)

Nicolas, M.P.B. 2007. Devonian Three Forks Formation, Manitoba (NTS 62F, parts of

    62G, K): preliminary hydrocarbon and stratigraphic investigations.

Nordeng, S. H., 2010, The Bakken source system: Emphasis on the Three Forks

    Formation: 18th Williston Basin Petroleum Conference and Expo, North Dakota

    Geological Survey, *PowerPoint presentation*.

North Dakota Geological Survey—*Wilson M. Laird Core & Sample Library, Grand Forks,*

    ND, USA, 2013.

Peterson, J. A., and I. M. MacCary, 1987, Regional stratigraphy and general petroleum

    geology of the U.S. portion of the Williston Basin and adjacent areas, in M. W.

    Longman, ed., *Williston Basin: Anatomy of a Cratonic Oil Province: Denver,*

    Colorado, Rocky Mountain Association of Geologists, p. 9-43.

Ashu, R. 2014. Stratigraphy, depositional environments and petroleum potential of the

    Three Forks Formation—Williston Basin, North Dakota[Ph.D. thesis],University of

    North Dakota, Grand Forks, ND, USA, 2014.

Sandberg, C.A., and C.R. Hammond. 1958. Devonian system in Williston Basin and

        central Montana: *AAPG Bulletin,* v. 42, no. 10, p. 2293-2334.

Schembre, J.M., and A.R. Kovscek. 2006. Estimation of dynamic relative permeability

        and capillary pressure from countercurrent imbibition experiments. *Transp.*

        Porous Media, 65: 31-51.

Silin, D. and T. Kneafsey. 2012. Shale gas: Nanometer-scale observations and well

        modelling. *J. Canad. Petrol. Technol.,* 51(6): 464-475.

Sloss, I. I. 1963. Sequences in the cratonic interior of the North America: *Geological*

        Society of America Bulletin, v. 74, p. 93-114.

SPE ATW (Society of Petroleum Engineers Applied Technology Workshop), 2013.

        Production Decline in Oil and Gas Shale Reservoirs: *What Can We do to*

        improve the Performance? 27 February – 1 March 2013, Santa Fe, New Mexico.

        http://www.spe.org/events/13asfe/.

Swanson, B. F. 1979. Visualizing pores and nonwetting phase in porous rock. *J. Petrol.*

        Technol., 31: 10–18.

Tran, T. 2011. Bakken Shale Oil Production Trends. *Masters' Thesis submitted to the*

        Office of Graduate Studies, Texas A&M University.

US Department of the Interior, USGS Releases of New Oil and Gas Assessment for

        Bakken and Three Forks, 30 Apr. 2013.

Wang, D., R. Butler, H. Liu, and S. Ahmed. 2010. Flowrate Behavior and Imbibition in

        Shale. SPE 138521. *Presented at the SPE regional meeting in West Virginia,*

        October 2010.

Wang, D., R. Butler, J. Zhang, and R. Seright. 2012. Wettability Survey in Bakken Shale

        with Surfactant-formulation Imbibition, *SPE Reserv. Eval. & Eng.* 15(, 6): 695-

        705.

Zhou, J.A., G.A. Ye, and K. van Breugel. 2010. Characterization of pore structure in cement-based materials using pressurization-depressurization cycling mercury intrusion porosimetry (PDC-MIP). *Cement Conc. Res.*, 40(7): 1120-1128.

Biographical Information

Daniel Samuel Baah obtained his Bachelors of Science in Geology from the University of Ghana, Accra, Ghana in 2011, and Masters of Science in Geology from University of Texas at Arlington in 2015. His research interest while at University of Texas at Arlington was focused on using multiple approaches to characterize the pore structure of the Three Forks Formation in the Williston Basin, North Dakota reservoir. After graduation Daniel intends to work in the oil and gas industry, preferably in exploration.